

RESEARCH ARTICLE

# Coculture with Colon-26 cancer cells decreases the protein synthesis rate and shifts energy metabolism toward glycolysis dominance in C2C12 myotubes

Yuki Tamura,<sup>1,3,5,6,7,8</sup> Karina Kouzaki,<sup>2,4,5</sup> Takaya Kotani,<sup>5,9</sup> and Koichi Nakazato<sup>2,3,4,5</sup>

<sup>1</sup>Faculty of Sport Science, Nippon Sport Science University, Tokyo, Japan; <sup>2</sup>Faculty of Medical Science, Nippon Sport Science University, Tokyo, Japan; <sup>3</sup>Graduate School of Health and Sport Science, Nippon Sport Science University, Tokyo, Japan; <sup>4</sup>Graduate School of Medical and Health Science, Nippon Sport Science University, Tokyo, Japan; <sup>5</sup>Research Institute for Sport Science, Nippon Sport Science University, Tokyo, Japan; <sup>6</sup>High Performance Center, Nippon Sport Science University, Tokyo, Japan; <sup>7</sup>Sport Training Center, Nippon Sport Science University, Tokyo, Japan; <sup>8</sup>Center for Coaching Excellence, Nippon Sport Science University, Tokyo, Japan; and <sup>9</sup>Department of Sports Sciences, The University of Tokyo, Tokyo, Japan

## Abstract

Cancer cachexia is the result of complex interorgan interactions initiated by cancer cells and changes in patient behavior such as decreased physical activity and energy intake. Therefore, it is crucial to distinguish between the direct and indirect effects of cancer cells on muscle mass regulation and bioenergetics to identify novel therapeutic targets. In this study, we investigated the direct effects of Colon-26 cancer cells on the molecular regulating machinery of muscle mass and its bioenergetics using a coculture system with C2C12 myotubes. Our results demonstrated that coculture with Colon-26 cells induced myotube atrophy and reduced skeletal muscle protein synthesis and its regulating mechanistic target of rapamycin complex 1 signal transduction. However, we did not observe any activating effects on protein degradation pathways including ubiquitin-proteasome and autophagy-lysosome systems. From a bioenergetic perspective, coculture with Colon-26 cells decreased the complex I-driven, but not complex II-driven, mitochondrial ATP production capacity, while increasing glycolytic enzyme activity and glycolytic metabolites, suggesting a shift in energy metabolism toward glycolysis dominance. Gene expression profiling by RNA sequencing showed that the increased activity of glycolytic enzymes was consistent with changes in gene expression. However, the decreased ATP production capacity of mitochondria was not in line with the gene expression. The potential direct interaction between cancer cells and skeletal muscle cells revealed in this study may contribute to a better fundamental understanding of the complex pathophysiology of cancer cachexia.

**NEW & NOTEWORTHY** We explored the potential direct interplay between colon cancer cells (Colon-26) and skeletal muscle cells (C2C12 myotubes) employing a noncontact coculture experimental model. Our findings reveal that coculturing with Colon-26 cells substantially impairs the protein synthesis rate, concurrently instigating a metabolic shift toward glycolytic dominance in C2C12 myotubes. This research unveils critical insights into the intricate cellular cross talk underpinning the complex pathophysiology of cancer cachexia.

C2C12; cancer cachexia; Colon-26; glycolysis; mitochondria

## INTRODUCTION

Cancer cachexia, a condition characterized by the atrophy of skeletal muscle and adipose tissue in association with cancer, is not entirely reversible through conventional nutritional support (1). Depending on the type and stage of cancer, cachexia affects between 20% and 80% of cancer patients (2). This cancer-induced skeletal muscle atrophy not only compromises quality of life and independence, but it also undermines the efficacy of chemotherapy and reduces life expectancy (3–5). Given these critical clinical implications, extensive research has been conducted in recent years, aiming to unravel the pathophysiology and pathogenesis of skeletal muscle atrophy due to cancer at the cellular and

molecular levels, as well as general muscle atrophy resulting from physical inactivity and aging.

Basic research on cancer cachexia often employs cancer-xenografted mouse models, such as the Colon-26 tumor-bearing mouse model, to investigate skeletal muscle mass and functions. The pathogenesis of cancer cachexia is complex because it occurs as a result of cross talk among various tissues and cell types (6, 7). In addition to the complex interorgan cross talk, patient behavioral changes, such as decreased physical activity and energy intake, are also modifiers of the disease state (8). Therefore, understanding cancer cachexia comprehensively as a single biological system, mainly in animal models, and resolving the complex multifactorial interactions stepwise are needed to elucidate its pathogenesis.



In vitro approaches, such as adding Colon-26 cell-conditioned medium to C2C12 myotube culture medium, have been adopted to evaluate direct interactions between cancer cells and skeletal muscle cells through humoral factors (9, 10). These methods have reproduced the major phenotypes of in vivo cachexia models, such as myotube atrophy. Furthermore, it has been recently shown that coculture of Colon-26 cells and C2C12 myotubes induces greater myotube atrophy than supplying conditioned medium (11). Therefore, drug screening for cancer cachexia has been conducted using cocultures of Colon-26 cells and C2C12 myotubes (12–14). However, although myotube atrophy occurs in coculture with Colon-26 cells, there is insufficient understanding of whether the molecular mechanism controlling skeletal muscle size operates in the same manner as that in the in vivo cachexia models.

Emerging evidence has suggested that changes in energy metabolism of skeletal muscle are significant factors in the pathogenesis of cachexia (15, 16). For example, cancer cachexia impairs mitochondrion-centered oxidative metabolism (17–20). Interestingly, it is becoming clear that mitochondrial dysfunction associated with cancer cachexia is a consequence as well as a cause or exacerbator of cancer cachexia (21). However, it remains unclear whether the changes in energy metabolism caused by cancer cachexia are directly induced by cancer cells or whether they are the result of contributions from other cell types or changes in patient behavior.

To further understand the pathophysiology and pathogenesis of cancer cachexia, we examined the potential direct effects of coculture with Colon-26 cells on pathways involved in protein metabolism and bioenergetics in C2C12 myotubes. We also profiled gene expression and examined whether the variations were consistent with signal transduction and downstream phenotypes.

## MATERIALS AND METHODS

### C2C12 Cell Culture

C2C12 myoblasts were purchased from the European Collection of Authenticated Cell Cultures (lot: 15E026). Cells were seeded on a standard 6-well culture plate (3335, Corning, NY) and grown in Dulbecco's modified high-glucose Eagle's medium (DMEM; 048-29763, Fujifilm Wako Pure Chemical Corporation, Osaka, Japan) without sodium pyruvate and containing 10% heat-inactivated fetal bovine serum (FBS; 12483-020, Thermo Fisher Scientific, Waltham, MA) and 1% penicillin-streptomycin (P/S; 168-23191, Fujifilm Wako Pure Chemical Corporation). At ~90% confluence, the medium was replaced with differentiation medium [high-glucose DMEM without sodium pyruvate and containing 2% heat-inactivated horse serum (16050122, Thermo Fisher Scientific) and 1% P/S]. The differentiation profiles of C2C12 cells used in this study are shown in Supplemental Fig. S1 (all Supplemental figures are available at <https://doi.org/10.6084/m9.figshare.25426069.v3>).

### Colon-26 Cell Culture

Colon-26-Luc cells were purchased from the Japanese Collection of Research Bioresources Cell Bank (JCRB1496,

lot: 11022012). Cells were seeded on a culture insert in a 6-well plate (353102, Corning) and grown in proliferation medium (high-glucose DMEM, 10% FBS, 1% P/S, without sodium pyruvate). As a preliminary experiment, the Colon-26 cells used in this study were confirmed to induce typical cachexia symptoms, such as weight loss and skeletal muscle atrophy, when transplanted into 8-wk-old male Balb/c mice ( $1 \times 10^6$  Colon-26 cells, 2 wk). The results of the validation are shown in Supplemental Fig. S2. Animal experiments were approved by the Animal Experimental Committee of Nippon Sport Science University (Approval No. O18-A03) and complied with the policies and regulations of the *Fundamental Guidelines for Proper Conduct of Animal Experiments and Related Activities in Academic Research Institutions* published by the Ministry of Education, Culture, Sports, Science and Technology, Japan (No. 71, 2006).

### Primary Colon Epithelial Cells Culture

Isolation and culture of colon epithelial cells were performed as described previously (22). Six-week-old female BALB/c mice were euthanized via cervical dislocation, and their colons were harvested. The colons were longitudinally opened and rinsed with phosphate-buffered saline (PBS) to remove contents. Colon tissues were then cut into 2-mm<sup>2</sup> pieces and incubated in PBS containing 3 mM EDTA and 0.5 mM DTT for 1 h at 4°C. After incubation, the tissue pieces were washed with PBS and vigorously shaken for 30 s to dislodge crypts. The freed crypts were collected by centrifugation (500 g, 5 min, 22°C) and resuspended in proliferation medium [DMEM (high glucose), 1 µg/mL insulin, 20% FBS, and 1% P/S]. Between 100 and 200 crypts were seeded into each well of a 24-well plate coated with collagen I. After 48 h, crypts that had adhered to the bottom and begun to migrate were reseeded into 25-cm<sup>2</sup> flasks. Fibroblasts were removed by exploiting the differential trypsin sensitivity between epithelial cells and fibroblasts (24). Five minutes after trypsinization, the solution was removed, and the remaining cells were cultured as epithelial cells. This selection process was repeated at least three times during proliferation. For coculturing with C2C12 myotubes, cells were seeded onto cell culture inserts previously coated with collagen I.

### Noncontact Coculture of C2C12 Myotubes and Colon-26 Cells/Primary Epithelial Cells

Seventy-two hours after the start of differentiation into C2C12 myotubes, culture inserts (1-µm pore size) with Colon-26 or primary epithelial cells were placed in 6-well plates containing C2C12 myotubes. Differentiation medium was used for coculture. Seventy-two hours after the start of coculture, the cells were collected and subjected to various assays. The medium volume was 0.263 mL/cm<sup>2</sup> of culture surface area [1 well (9.5 cm<sup>2</sup>) of a 6-well plate: 2.5 mL; 1 cell culture insert (4.2 cm<sup>2</sup>): 1.1 mL]. The scheme of the coculture procedure and images of the equipment used are shown in Fig. 1.

### Protein Extraction and Western Blotting

Protein extraction and Western blot analysis were performed as described previously (23, 25). Briefly, cells were homogenized in RIPA buffer (188-02453, Fujifilm Wako Pure Chemical Corporation) containing a protease and phosphate

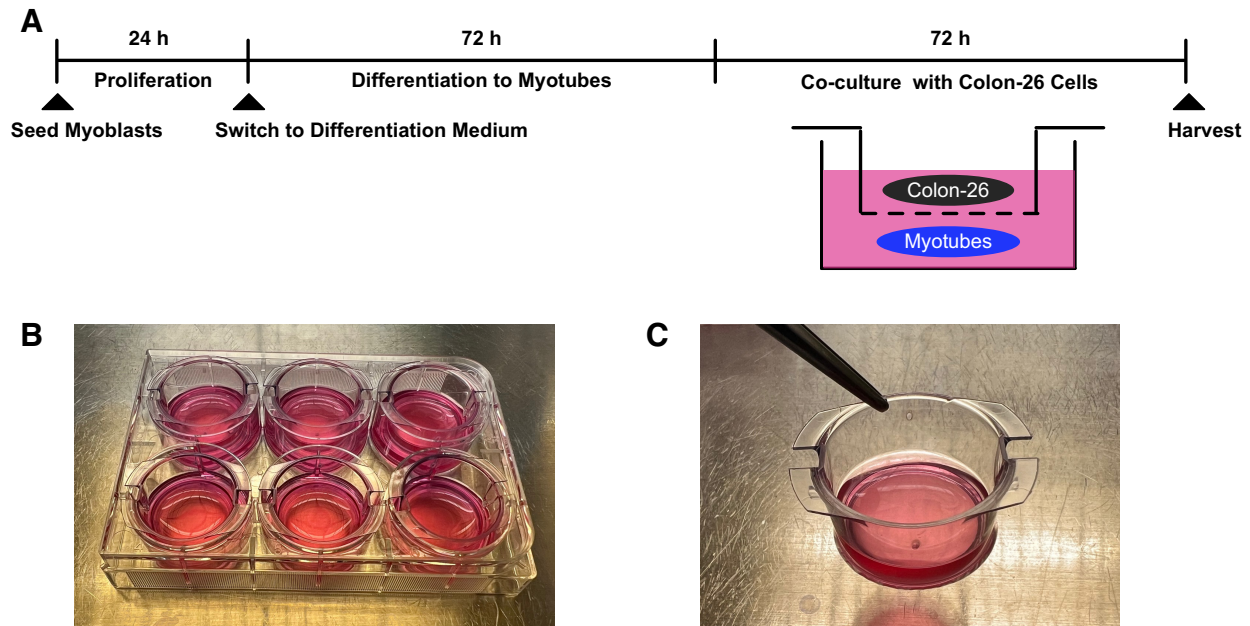


**Figure 1.** Experimental procedure and equipment used in this study are shown. *A*: schematic illustration of the step-by-step experimental procedure utilized in this study. *B* and *C*: noncontact coculture methodology employed using cell culture inserts, highlighting the technical setup and arrangement of the cell culture system.

inhibitor cocktail (169-26063/167-24381, Fujifilm Wako Pure Chemical Corporation). The protein concentration was measured using a BCA assay (295-78401, Fujifilm Wako Pure Chemical Corporation). Equal amounts of protein (10  $\mu$ g) were separated by SDS-PAGE [10% and 12% (wt/vol) TGX polyacrylamide gels (161-0173/161-0175, Bio-Rad, Hercules, CA)] and transferred to a polyvinylidene difluoride membrane (IPVH00010, Merck Millipore, Burlington, MA). Protein transfer was confirmed by staining with Ponceau S (33427.01, SERVA Electrophoresis, Heidelberg, Germany). The membrane was blocked with a blocking reagent (NYPBR01, Toyobo Co., Osaka, Japan) for 1 h and incubated with a primary antibody diluted in Can Get Signal reagent 1 (NKB-101, Toyobo Co.) for 1 h. The antibodies used in this study are listed in Supplemental Table S1 (all Supplemental tables are available at <https://doi.org/10.6084/m9.figshare.23574276.v1>). After incubation, the membrane was washed with Tris-buffered saline containing 0.01% Tween 20 (T9142, Takara Bio Inc., Shiga, Japan). Then membrane was then incubated with a secondary antibody (7074/7076, Cell Signaling Technology, Danvers, MA) diluted in Can Get Signal reagent 2 (NKB-101, Toyobo Co.) for 1 h at room temperature and washed again with Tris-buffered saline containing 0.01% Tween 20. Chemiluminescent reagents (SuperSignal West Pico Chemiluminescent Substrate; Thermo Fisher Scientific) were used for development. Blots were scanned and quantified using a ChemiDoc XRS (170-8071, Bio-Rad) and Quantity One software (170-9600, version 4.5.2, Windows, Bio-Rad). The Ponceau S signal intensity (37–75 kDa) was used as the loading control.

### Protein Synthesis Rate Assay

Protein synthesis rate was measured with SUNSET method (26). Puromycin (160-23151, Fujifilm Wako Pure Chemical Corporation) at a final concentration of 1  $\mu$ M was added to

culture medium at 30 min before cells were harvested. Proteins were extracted as described above, and samples were prepared for Western blotting. An antibody against puromycin was used to measure the amount of proteins incorporating puromycin. The signal intensity between 25 and 150 kDa was quantified.

### Autophagic Flux Assay

Autophagic flux was measured as previously described with minor modifications (27). Bafilomycin A1 (19-148, Merck Millipore) at a final concentration of 100 nM was added to culture medium at 3 h before collecting cells. Proteins were extracted as described above, and samples were prepared for Western blotting. Protein levels were determined using an anti-LC3-II antibody.

### DNA Extraction

C2C12 myotubes were washed with PBS, and DNA was extracted using a commercial DNA extraction kit (Dneasy Blood & Tissue Kit, 69504, Qiagen).

### RNA Extraction

RNA samples were prepared as described previously (28, 29). C2C12 myotubes were homogenized in TRIzol reagent (Thermo Fisher Scientific) on ice and separated into organic and aqueous phases using chloroform. RNA was isolated from the aqueous phase following precipitation with ethanol with a commercial kit (FG-80050, Nippon Genetics, Tokyo, Japan). The RNA concentration and purity were measured by spectrophotometry (Nanodrop One, Thermo Fisher Scientific).

### Real-Time Quantitative PCR

Expression of genes of interest was quantified using a quantitative PCR reagent (QPS-201, Toyobo Co.) and a

thermal cycler with an optical reaction module (CFX96 Touch, Bio-Rad). Samples were analyzed in duplicate simultaneously with a negative control without cDNA. *Tbp* (TATA-binding protein) was used as a housekeeping gene, the expression of which was not statistically different between groups ( $P = 0.89$ ). Mitochondrial DNA copy number assays were performed as described (30). The primer sequences used are shown in Supplemental Table S2 (<https://doi.org/10.6084/m9.figshare.23574276.v1>). Primer specificity was confirmed by a dissociation curve in each PCR and electrophoresis after PCR. Quantification was performed using the calibration curve method (31).

### Library Preparation, RNA-Seq, and Bioinformatics Analyses

Sequencing libraries for gene expression profiling (3' mRNA-seq) were prepared using a commercial kit (QuantSeq 3' mRNA-seq Library Prep Kit FWD for Illumina, Lexogen, Inc., Vienna, Austria). First-strand DNA was synthesized from 2  $\mu$ g RNA template with oligodT primers containing the Illumina-specific Read2 linker sequence. After removal of the RNA template, the second strand was synthesized using random primers containing the Illumina-specific Read1 linker sequence. Double-stranded cDNA libraries were washed and purified with magnetic beads. After purification, the libraries were amplified by PCR with primers containing an adaptor and the i7 index sequence. Libraries were purified with magnetic beads, quantified using a fluorometer (Qubit 4, Thermo Fisher Scientific), and pooled by adjusting to an equimolar concentration.

Sequencing was performed using a MiniSeq High Output Reagent Kit (75 cycles) on a MiniSeq system (Illumina, San Diego, CA). After sequencing, the sequencing quality was examined using FastQC. Adaptor sequences and the polyA sequence were trimmed using cutadapt and mapped to the reference sequence using Salmon, and the read number was counted. Data of raw read counts from each sample were normalized by the rlog algorithm (gene median; minimal counts per million: 0.5). Further bioinformatics were conducted by integrated differential expression and pathway analysis (10). Differential gene expression analyses were conducted using DESeq2 (false discovery rate cutoff: 0.10; minimal fold change: 2.0). Pathway enrichment analyses were performed using three independent gene sets, namely Gene Ontology (Go; biological processes), Kyoto Encyclopedia of Genes and Genomes (KEGG), and Reactome. For pathway analysis, genes that passed through the filter were used as background.

### Live Cell Imaging

Live cell imaging was performed as described previously (32). Myotubes were washed in PBS twice and loaded with fluorescent dyes [nuclear: Hoechst 33342 [excitation (Ex): 342 nm/emission (Em): 461 nm, 346-07951, Dojindo Molecular Technology Inc., Kumamoto, Japan]; whole cell: calcein AM solution (Ex: 490 nm/Em: 515 nm, C396, Dojindo Molecular Technology Inc.), MitoBright Red solution (Ex: 547 nm/Em: 563 nm, MT007, Dojindo Molecular Technology Inc.), JC-1 mitochondrial membrane potential detection solution (Ex1: 490 nm/Em1: 515 nm, Ex2: 547 nm/Em2: 563 nm, MT007,

Dojindo Molecular Technology Inc.), and MitoSOX Red Mitochondrial superoxide indicator (Ex: 396 nm/Em: 610 nm, M36005, Thermo Fisher Scientific)] following the manufacturers' instructions. Cells were washed in PBS twice and imaged under a confocal laser scanning microscope (FV3000, Olympus, Tokyo, Japan). Fluorescent intensities were quantified using ImageJ (Ver. 2.3.0, Mac).

### Myotube Diameter Measurement

One hundred myotubes stained with Calcein AM were randomly selected, and their diameters were measured by ImageJ.

### Mitochondrial Respiration Assay

Mitochondrial respiration was measured as described previously (32). C2C12 myotubes were harvested using trypsin-EDTA (209-16941, Fujifilm Wako Pure Chemical Corporation) and gently resuspended in reaction buffer (0.5  $\mu$ g/mL digitonin, 105 mM potassium-MES, 10 mM Tris, 30 mM KCl, 10 mM  $\text{KH}_2\text{PO}_4$ , 5 mM  $\text{MgCl}_2$ , 1 mM EGTA, and 2.5 g/L BSA, pH 7.2). Mitochondrial oxygen consumption was measured using a multimode plate reader (Spark 20 M, Tecan) with oxygen monitoring on a 96-well microplate (OP96C, PreScan Precision Sensing, Regensburg, Germany) (Ex: 540 nm/Em: 650 nm). The substrates used to measure the mitochondrial oxygen consumption rate were 10 mM pyruvate (29805-22, Nacalai Tesque, Kyoto, Japan) + 5 mM malate (138-07512, Fujifilm Wako Pure Chemical Corporation), 10 mM glutamate (072-00501, Fujifilm Wako Pure Chemical Corporation) + 5 mM malate, 200  $\mu$ M octanoylcarnitine (50892, Sigma-Aldrich) + 5 mM malate, and 10 mM succinate (199-03305, Fujifilm Wako Pure Chemical Corporation) + 0.5  $\mu$ M rotenone (599-10811, Fujifilm Wako Pure Chemical Corporation). To induce ATP production-coupled respiration (state 3), 2.5 mM ADP (01652-24, Nacalai Tesque) were added. After the sample and assay solutions were mixed, the mineral oil was used to cover the top to prevent oxygen from the air from dissolving into the solution. The relative change in fluorescence per minute was measured and converted to the oxygen consumption rate in accordance with the manufacturer's instructions. Relative fluorescence changes were measured per minute and normalized to the protein content.

### Enzymatic Activity Assays

Cells were homogenized in buffer (250 mM sucrose, 50 mM Tris, and 5 mM  $\text{MgCl}_2$ , pH 7.4). Protein concentrations were determined by the BCA assay and adjusted to 1 mg/mL.

A creatine kinase activity assay was performed as described previously with minor modifications (33). Ten micrograms of protein were mixed with reaction buffer [50 mM Tris-HCl, 2.5 mM ADP, 10 mM  $\text{MgCl}_2$ , 30 mM phosphocreatine (032-04583, Fujifilm Wako Pure Chemical Corporation), 30 mM glucose (132-001751, Fujifilm Wako Pure Chemical Corporation), 1 mM  $\text{NADP}^+$  (308-50463, Fujifilm Wako Pure Chemical Corporation), 20 mM NAC (015-05132, Fujifilm Wako Pure Chemical Corporation), 2 mM EDTA (345-01865, Fujifilm Wako Pure Chemical Corporation), 1 mM AMP (303-50491, Fujifilm Wako Pure Chemical Corporation), 1 U/ $\mu$ L glucose-6-phosphate dehydrogenase (074-04101, Fujifilm Wako Pure Chemical Corporation), and 3 U/ $\mu$ L hexokinase

(302-51681, Fujifilm Wako Pure Chemical Corporation), pH 8.0] in a 96-well plate. Absorbance changes at 340 nm/min were calculated.

An adenylate kinase activity assay was performed as described previously with minor modifications (33). Ten micrograms of protein were mixed with reaction buffer (50 mM Tris·HCl, 2.5 mM ADP, 10 mM MgCl<sub>2</sub>, 30 mM glucose, 1 mM NADP<sup>+</sup>, 1 U/μL glucose-6-phosphate dehydrogenase, and 3 U/μL hexokinase, pH 8.0) in a 96-well plate. Absorbance changes at 340 nm/min were calculated.

A hexokinase activity assay was performed as described previously with minor modifications (34). Ten micrograms of protein were mixed with reaction buffer (50 mM Tris·HCl, 1 mM ATP, 10 mM MgCl<sub>2</sub>, 30 mM glucose, 1 mM NADP<sup>+</sup>, and 1 U/μL glucose-6-phosphate dehydrogenase, pH 8.0) in a 96-well plate. Absorbance changes at 340 nm/min were calculated.

A glycogen phosphorylase activity assay was performed as described previously (35). Ten micrograms of protein were mixed with reaction buffer [20 mM PIPES (348-08251, Fujifilm Wako Pure Chemical Corporation), 0.8% glycogen (074-05561, Fujifilm Wako Pure Chemical Corporation), 50 mM sodium phosphate, 200 μM NADP<sup>+</sup>, 500 μM glucose-1,6-bisphosphate (G6893, Sigma-Aldrich), 1 U/μL glucose-6-phosphate dehydrogenase, and 3 U/μL phosphoglucomutase (P3397, Sigma-Aldrich), pH 8.0] in a 96-well plate. Absorbance changes at 340 nm/min were calculated.

A phosphofructokinase activity assay was performed as described previously with minor modifications (34). Ten micrograms of protein were mixed with reaction buffer [10 mM Tris·HCl, 1 mM ATP, 7 mM phosphoenolpyruvate (160-14763, Fujifilm Wako Pure Chemical Corporation), 200 μM NADH (305-50451, Fujifilm Wako Pure Chemical Corporation), 10 mM fructose-6-phosphate (066-05341, Fujifilm Wako Pure Chemical Corporation), 5 μM KCl, 2 mM MgSO<sub>4</sub>, 1 U/μL pyruvate kinase (305-50711, Fujifilm Wako Pure Chemical Corporation), and 1 U/μL lactate dehydrogenase (300-52721, Fujifilm Wako Pure Chemical Corporation), pH 8.0] in a 96-well plate. Absorbance changes at 340 nm/min were calculated.

A pyruvate kinase activity assay was performed as described previously with minor modifications (36). Ten micrograms of protein were mixed with reaction buffer (50 mM HEPES, 100 mM MgCl<sub>2</sub>, 5 μM KCl, 7 mM phosphoenolpyruvate, 200 μM NADH, 2.5 mM ADP, and 1 U/μL lactate dehydrogenase, pH 8.0) in a 96-well plate. Absorbance changes at 340 nm/min were calculated.

A lactate dehydrogenase (pyruvate to lactate) activity assay was performed as described previously (32). Ten micrograms of protein were mixed with reaction buffer [50 mM Tris·HCl, 10 mM sodium pyruvate (195-05965, Fujifilm Wako Pure Chemical Corporation), and 200 μM NADH, pH 8.0] in a 96-well plate. Absorbance changes at 340 nm/min were calculated.

To measure pyruvate dehydrogenase activity, 10 μg of protein were mixed with reaction buffer [100 mM Tris·HCl, 200 μM thiamine pyrophosphate (T10183, Tokyo Chemical Industry, Tokyo, Japan), 2.5 mM NAD<sup>+</sup>, 100 μM CoA-SH (302-50483, Fujifilm Wako Pure Chemical Corporation), 10 mM sodium pyruvate, 10 mM MgCl<sub>2</sub>, 0.01% Triton X-100, 50 μM 1-methoxy-5-methylphenazinium methylsulfate

(341-04003, Fujifilm Wako Pure Chemical Corporation), and 100 μM WST-3 (345-08881, Fujifilm Wako Pure Chemical Corporation), pH 8.0] in a 96-well plate. Absorbance changes at 433 nm/min were calculated.

A citrate synthase activity assay was performed as described previously (37). Ten micrograms of protein were mixed with reaction buffer [50 mM Tris·HCl, 100 μM DTNB (346-08551, Dojindo Molecular Technologies, Inc.), 300 μM acetyl-CoA (00546-54, Nacalai Tesque), 50 μM oxaloacetate (25804-81, Nacalai Tesque), and 0.01% Triton X-100, pH 7.4] in a 96-well plate. Absorbance changes at 412 nm/min were calculated.

An isocitrate dehydrogenase activity assay was performed as described previously with minor modifications (38). Ten micrograms of protein were mixed with reaction buffer [100 mM Tris·HCl, 5 mM isocitrate (19608-51, Nacalai Tesque), 1 mM NAD<sup>+</sup>, and 10 mM MgCl<sub>2</sub>, pH 8.0] in a 96-well plate. Absorbance changes at 340 nm/min were calculated.

An α-ketoglutarate dehydrogenase activity assay was performed as described previously with minor modifications (39). Ten micrograms of protein were mixed with reaction buffer [100 mM Tris·HCl, 200 μM thiamine pyrophosphate, 2.5 mM NAD<sup>+</sup>, 100 μM CoA-SH, 10 mM α-ketoglutarate (19817-82, Nacalai Tesque), 10 mM MgCl<sub>2</sub>, 0.01% Triton X-100, 50 μM 1-methoxy-5-methylphenazinium methylsulfate, and 100 μM WST-3, pH 8.0] in a 96-well plate. Absorbance changes at 433 nm/min were calculated.

A succinate dehydrogenase (complex II) activity assay was performed as described previously (40). Ten micrograms of protein were mixed with reaction buffer [20 mM succinate, 0.015% (wt/vol) 2,6-dichlorophenolindophenol (591-03541, Fujifilm Wako Pure Chemical Corporation), 12.5 μM decylubiquinone (195-041, 599-10811, Fujifilm Wako Pure Chemical Corporation), 300 μM KCN, and 1 mg/mL BSA] in a 96-well plate. Absorbance changes at 600 nm/min were calculated.

To measure malate dehydrogenase, 10 μg of protein were mixed with reaction buffer [100 mM Tris·HCl, 5 mM malate, 1 mM NAD<sup>+</sup>, and 10 mM MgCl<sub>2</sub>, pH 8.0] in a 96-well plate. Absorbance changes at 340 nm/min were calculated.

A complex I activity assay was performed as described previously (40). Ten micrograms of the protein suspension were mixed with reaction buffer [100 μM NADH, 60 μM ubiquinone (C7956, Sigma-Aldrich, St. Louis, MO), 300 μM KCN, and 3 mg/mL BSA] in a 96-well plate. Absorbance changes at 340 nm were calculated every minute. Rotenone-sensitive enzyme activity (i.e., rotenone absence - rotenone presence) was regarded as complex I activity.

A complex I + III activity assay was performed as described previously (40). Ten micrograms of protein were mixed with reaction buffer [200 μM NADH, 50 μM cytochrome *c* (C2506, Sigma-Aldrich), 300 μM KCN, and 1 mg/mL BSA] in a 96-well plate. Absorbance changes at 550 nm/min were calculated.

A complex II + III activity assay was performed as described previously (40). Ten micrograms of protein were mixed with reaction buffer (10 mM succinate, 50 μM cytochrome *c*, and 300 μM KCN) in a 96-well plate. Absorbance changes at 550 nm/min were calculated.

A complex IV activity assay was performed as described previously with minor modifications (41). Ten micrograms of protein were mixed with reaction buffer (50 μM cytochrome

c reduced with dithiothreitol) in a 96-well plate. Absorbance changes at 550 nm/min were calculated.

### Mitochondrial Supercomplex Assembly

Mitochondrial supercomplex assembly was evaluated as described previously (40). Two-dimensional-PAGE [blue native (BN)-PAGE followed by SDS-PAGE] was conducted to evaluate mitochondrial supercomplex assembly. Isolated mitochondrial fractions (50 µg) were mixed with 5% digitonin (digitonin/protein ratio: 8 g/g; BN2006, Thermo Fisher Scientific) and 4× sample buffer (BN20032, Thermo Fisher Scientific) and incubated for 30 min on ice. After incubation, the suspensions were centrifuged at 20,000 g for 15 min at 4°C. Supernatants were collected, and a 5% Coomassie G-250 sample additive was applied (BN2004, Thermo Fisher Scientific). Proteins were loaded on 4%–20% gradient gels (4561096, Bio-Rad), and BN-PAGE was performed using buffers for native PAGE (BN2001, Thermo Fisher Scientific). BN-PAGE was followed by SDS-PAGE, and then proteins were transferred to a polyvinylidene difluoride membrane. Standard Western blot analysis was performed as described above using an anti-OXPHOS antibody [primary: ab110413 (1:1,000), Abcam, Cambridge, MA; secondary: 7076, Cell Signaling Technology].

### Glycogen Concentration Assay

A glycogen concentration assay was performed as described previously with minor modifications (32). Myotubes were collected in PBS and centrifuged at 600 g for 5 min. Supernatants were discarded, and the cell pellet was weighed. Cell pellets were resuspended in KOH saturated with NaSO<sub>4</sub> and incubated at 95°C. Ethanol was added to the resuspension, the resuspension was centrifuged, and the supernatant was discarded. Pellets were incubated at 37°C for 1 h to evaporate the supernatant. Pellets were resuspended in HCl and incubated at 95°C for 2 h to convert glycogen into glucose. The glucose concentration in the suspension was measured using a commercial kit (298-65701, Fujifilm Wako Pure Chemical Corporation).

### Sample Preparation for Intracellular Metabolite Measurements

C2C12 myotubes were disrupted by sonication (Biorupter, high, 30 s on and 30 s off, 15 cycles) in 0.6 N HClO<sub>4</sub> buffer. Centrifugation was performed at 12,000 g for 15 min at 4°C, and the supernatant was collected. The supernatant was neutralized using 1 M NaOH. Samples were analyzed to measure ATP, glucose-6-phosphate, pyruvate, and lactate.

### ATP Concentration Assay

The ATP concentration in cells was measured using a luminescence-based commercial kit (CellTiter-Glo 2.0 Cell Viability Assay, Promega).

### Glucose Concentration Assay

The glucose concentration in the culture medium was measured using a glucose oxidase-based commercial kit (298-65701, Fujifilm Wako Pure Chemical Corporation).

### Glucose-6-Phosphate Concentration Assay

A glucose-6-phosphate concentration assay of cells was performed as described previously with minor modifications (42). Briefly, 10 µL of standard glucose-6-phosphate solution or sample were incubated with 90 µL of reaction buffer (50 mM Tris·HCl, 20 µM MgCl<sub>2</sub>, 25 µM NADP<sup>+</sup>, 0.5 mM WST-3, 10 µM 1-methoxy-5-methylphenazinium methylsulfate, and 1 U/µL glucose-6-phosphate dehydrogenase, pH 8.0). Absorbance at 433 nm was measured after incubation for 30 min at room temperature in the dark.

### Pyruvate Concentration Assay

A pyruvate concentration assay of cells was performed as described previously with minor modifications (43). Briefly, 10 µL of standard sodium pyruvate solution or sample were incubated with 90 µL of reaction buffer (100 mM potassium phosphate with 1.0 mM EDTA, pH 6.7, 1.0 mM MgCl<sub>2</sub>, 10 µM FAD, 0.2 mM thiamine pyrophosphate, 200 U/µL pyruvate oxidase, 50 µM Amplex red, and 200 U/µL horseradish peroxidase). After incubation for 30 min at room temperature in the dark, fluorescence at 590 nm was measured at an excitation of 535 nm using a microplate reader (Spark).

### Lactate Concentration Assay

A lactate concentration assay of culture medium and cell lysates was performed as described previously (32). Briefly, 10 µL of the standard sodium lactate solution or cell culture medium were incubated with 90 µL of the reaction buffer [2 U/mL lactate dehydrogenase (LDH), 0.4 M hydrazine, and 2.5 mM NAD<sup>+</sup>, pH 9.0]. After completion of the NAD<sup>+</sup> reducing reaction, which was confirmed by kinetic analysis, the final absorbance at 340 nm was measured using the microplate reader.

### Lactate Dehydrogenase Isozyme Assay

A lactate dehydrogenase isozyme assay was performed as described previously (32). Cells were homogenized in buffer (250 mM sucrose, 50 mM Tris, and 5 mM MgCl<sub>2</sub>, pH 7.4). Protein concentrations were determined using the BCA assay and adjusted to 2 mg/mL. Protein suspensions were mixed with glycerol (final concentration: 10%) and bromophenol blue (final concentration: 0.05 mg/mL). Equal amounts of protein (30 µg) were separated by native PAGE [7.5% (wt/vol) TGX polyacrylamide gels] at 12 mV for 100 min. After electrophoresis, gels were incubated in reaction buffer (1 M sodium lactate, 10 mM NAD<sup>+</sup>, 2 mg/mL phenazine-methosulphate, and 20 mg/mL tetrazolium blue) at 37°C until band development. Heart and quadriceps muscles obtained from C57BL/6J mice were used as positive controls.

### Mitochondrial ATP Assay

A fluorescent ATP biosensor Malion Red plasmid was obtained from Addgene (no. 113908) (44). Mitochondrial ATP levels were measured by modifying the ATP biosensor [addition of a mitochondrial localization signal (MSVLTPLLL-RGLTGSARRLPVPRAKIHSL) to the NH<sub>2</sub>-terminus of Malion Red, removing the COOH-terminal stop codon, and adding a T2A linker]. Downstream of the T2A linker, enhanced green fluorescent protein (EGFP) with a mitochondrial localization

signal added to the NH<sub>2</sub> terminus was joined and subcloned into an adeno-associated virus (AAV) plasmid with a CMV promoter, polyA signal, and WPRE sequence. The full sequence of this plasmid is provided in Supplemental Document S1 (<https://doi.org/10.6084/m9.figshare.23574279.v1>). After sequence confirmation by Sanger sequencing, competent cells (C3040, Stable, New England Biolabs, Ipswich, MA) were transformed with the plasmid and incubated in liquid medium (08246-44, Nacalai Tesque) at 30°C for 16 h with vigorous shaking. The plasmids were then extracted and purified, and intact ITR sequences for AAV packaging were confirmed by incubation with restriction enzyme SmaI (R0141S, New England Biolabs) and agarose electrophoresis.

For AAV packaging, HEK293T cells were cultured to 80% confluence. The AAV expression plasmid, AAV Rep/Cap plasmid (serotype 9), and AAV helper plasmid were cotransfected into HEK293T cells using PEI (23966-100, Polysciences, Warrington, PA). One day later, the medium was replaced with AAV production medium (10 mM HEPES, 0.075% sodium bicarbonate, and 1× Glutamax in low-glucose DMEM), and the cells were cultured for 5 days. AAV was isolated and purified in accordance with published methods (45, 46). AAV was quantified using a commercially available kit. AAV purity was determined by SDS-PAGE and CBB staining to confirm the presence of VP1, VP2, and VP3 bands and the absence of impurities.

For gene transfer by the AAV, 5 × 10<sup>10</sup> vg AAV particles were added to each well of a six-well plate at the time of coculture. Seventy-two hours later, confocal laser scanning microscopy was used to obtain the mitochondrial location (Mito:EGFP) and mitochondrial ATP information (Mito:Malion Red), and the red fluorescence intensity was divided by the green fluorescence intensity to obtain the ATP concentration per mitochondrion. To ensure the validity of the mitochondrial ATP measurement, we confirmed that ADP stimulation increased mitochondrial ATP levels by an increase in fluorescence intensity. The validation is shown in Supplemental Fig. S3.

### Statistical Analysis

Data are expressed as means ± SD. Unless noted otherwise, each condition was analyzed in four to six experiments. The Mann-Whitney *U* test was used for nonparametric two-group comparisons. The Kruskal-Wallis test followed by Dunn's tests was performed for nonparametric three-group comparisons. Two-way ANOVA was performed for autophagic flux analysis (coculture × bafilomycin A1). Statistical significance was defined as *P* < 0.05. All statistical analyses were performed using Prism (Ver. 8.4.3, Mac, GraphPad).

## RESULTS

### Coculture of Colon-26 Cells and C2C12 Myotubes Decreases Protein Synthesis Signaling and the Myotube Diameter

Noncontact coculture with Colon-26 cells for 72 h shifted the histogram of myotube diameters to the left (Fig. 2, A and B). Coculture with Colon-26 also reduced the mean diameter of myotubes by 40.8% (Fig. 2C). These results indicated that

myotubes were indeed atrophied by humoral factors from Colon-26 cells.

Skeletal muscle size is determined by the net balance between protein synthesis and degradation rates. Hence, to understand the molecular basis of myotube atrophy caused by coculture with Colon-26 cells, we evaluated the Akt/mechanistic target of rapamycin complex 1 (mTORC1) cascade, which is a central pathway involved in protein synthesis. In our observations, the phosphorylation status of Akt, p70S6K, and rpS6 was reduced when cocultured with Colon-26 cells (Fig. 3A). These results indicated that intracellular signaling pathways involved in protein synthesis were attenuated by coculture with Colon-26 cells. Furthermore, consistent with these results, coculture with Colon-26 cells reduced the protein synthesis rate as assessed by the puromycin incorporation assay (Fig. 3B).

We next evaluated proteolytic systems such as autophagy-lysosome system and ubiquitin-proteasome systems. We first analyzed autophagic flux using bafilomycin A1 (an inhibitor of autophagosome-lysosome fusion). The results showed that LC3-II protein was reduced by coculture with Colon-26 cells in the presence or absence of bafilomycin A1 (Fig. 3C). These observations were interpreted as a decrease in autophagic activity upon coculture with Colon-26 cells. We subsequently evaluated proteins that regulate the initial process of autophagy induction (ULK1) and contribute to autophagosome nucleation (ATG13, Beclin1, and ATG14L) and autophagosome elongation (ATG5). While the ratio of ULK1 in its inactive form (phosphorylated at Ser757) to the total ULK1 protein remained consistent, the active form of ULK1 (phosphorylated at Ser555) showed an increased ratio to the total ULK1 protein under coculture conditions (Fig. 3D). Conversely, protein levels of Beclin1, ATG14L, and ATG5 decreased in the coculture setting, while the protein level of ATG13 remained unchanged (Fig. 3D). Given these observations, we suggest that the coculture-induced decline in autophagy activity might be indicative of diminished efficiency in the processes governing the nucleation or elongation of autophagosomes. On the other hand, mRNA expression levels of E3 ubiquitin ligases *Trim63* (MuRF1) and *Fbxo32* (Atrogin1) were not changed by coculture with Colon-26 cells (Fig. 3E). Additionally, no obvious changes in ubiquitin-conjugated proteins were observed (Fig. 3E).

Thus far, we examined the effects of coculture with Colon-26 cells on the diameter of C2C12 myotubes and its regulators. The results indicated that coculture with Colon-26 cells caused myotube atrophy, which was consistent with the decreased activity of signal transduction for protein synthesis, but not with adaptations of the proteolysis system. Therefore, atrophy of myotubes caused by coculture with Colon-26 cells may be primarily due to a decrease in the protein synthesis capacity.

### Coculture with Colon-26 Cells Increases Glycolytic Metabolites in C2C12 Myotubes

We next examined whether coculture with Colon-26 cells changed bioenergetics in C2C12 myotubes. We first measured the ATP concentration in whole cells. As a result, no significant changes were observed in the ATP concentration of C2C12 myotubes after coculture with Colon-26 cells (Fig. 4A).

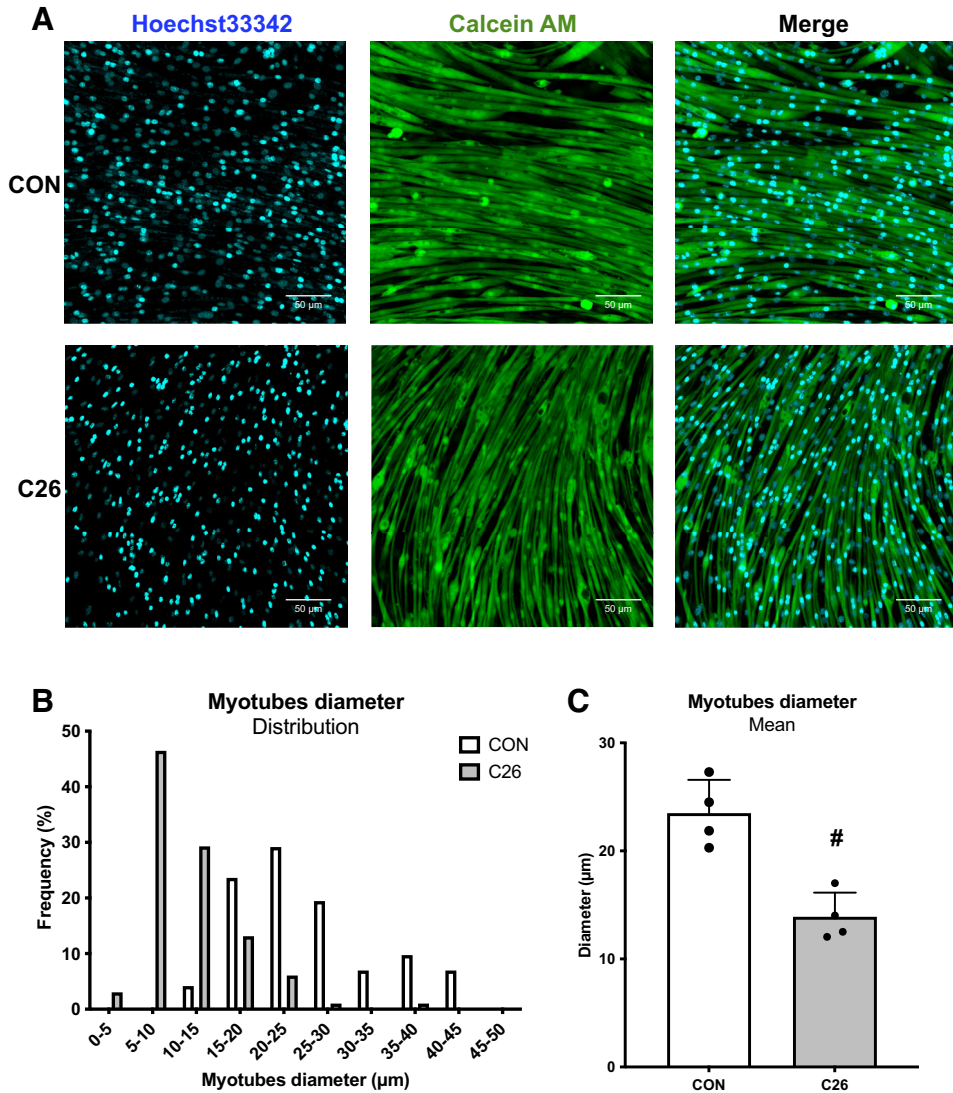


**Figure 2.** Coculture with Colon-26 cells induces atrophy of C2C12 myotubes. The effect of coculturing with Colon-26 cells on the atrophy of C2C12 myotubes is illustrated. **A:** representative image of the myotubes under investigation. **B:** histogram that visualizes the distribution of myotube diameters. **C:** mean myotube diameter, indicating significant atrophy with  $\#P < 0.05$  vs. the control (CON). Data are presented as means  $\pm$  SD.

However, coculture with Colon-26 cells decreased the mitochondrial ATP level (Fig. 4B). Next, we measured the concentration of metabolites related to glycolysis, such as glycogen, glucose-6-phosphate, pyruvate, and lactate, in C2C12 myotubes. Coculture did not cause any changes in the glycogen concentration, but the concentrations of glucose-6-phosphate, pyruvate, and lactate were increased in C2C12 myotubes (Fig. 4C).

After 72 h of monoculture or coculture, culture medium was collected and metabolites were measured. We observed the characteristic change in the culture medium where phenol red became yellow in coculture (Fig. 4D), despite adjusting the medium volume in accordance with the culture surface area. Additionally, we observed a decrease in the pH of the medium (Fig. 4E). Glucose utilization and the lactate concentration after 72 h of culture, which were adjusted to the culture surface area, were higher in cocultures of C2C12 myotubes and Colon-26 cells than in monocultures of C2C12 myotubes or Colon-26 cells (Fig. 4, F and G). However, we did not observe any significant changes in the concentrations of metabolites of glycolysis, including glucose-6-phosphate, pyruvate, and lactate, in Colon-26 cells, regardless of monoculture or

coculture (Supplemental Fig. S4A). Furthermore, we did not observe an increase in the glycolytic enzyme activity or a decrease in mitochondrial oxidative capacity of Colon-26 cells between solo-culture and coculture with C2C12 myotubes (Supplemental Fig. S4, B–F). These results suggested that changes in metabolites in the culture medium after coculture strongly reflected the metabolic changes in C2C12 myotubes, and remodeling of bioenergetic machinery (e.g., activation of the glycolytic system and/or failure of mitochondrial oxidative phosphorylation) may have occurred to maintain a constant intracellular ATP concentration.

#### Coculture with Colon-26 Does Not Affect Creatine or Adenylate Kinases in C2C12 Myotubes

We next examined whether the energy system adapted to coculture with Colon-26 cells. Specifically, we evaluated the phosphagen system, glycolytic system, pyruvate and lactate metabolisms, and mitochondrial oxidative phosphorylation. We then evaluated the activity of creatine kinase and adenylate kinases in the phosphagen system. No changes were observed in any of these metabolic enzymes after coculture with Colon-26 cells (Fig. 5A).

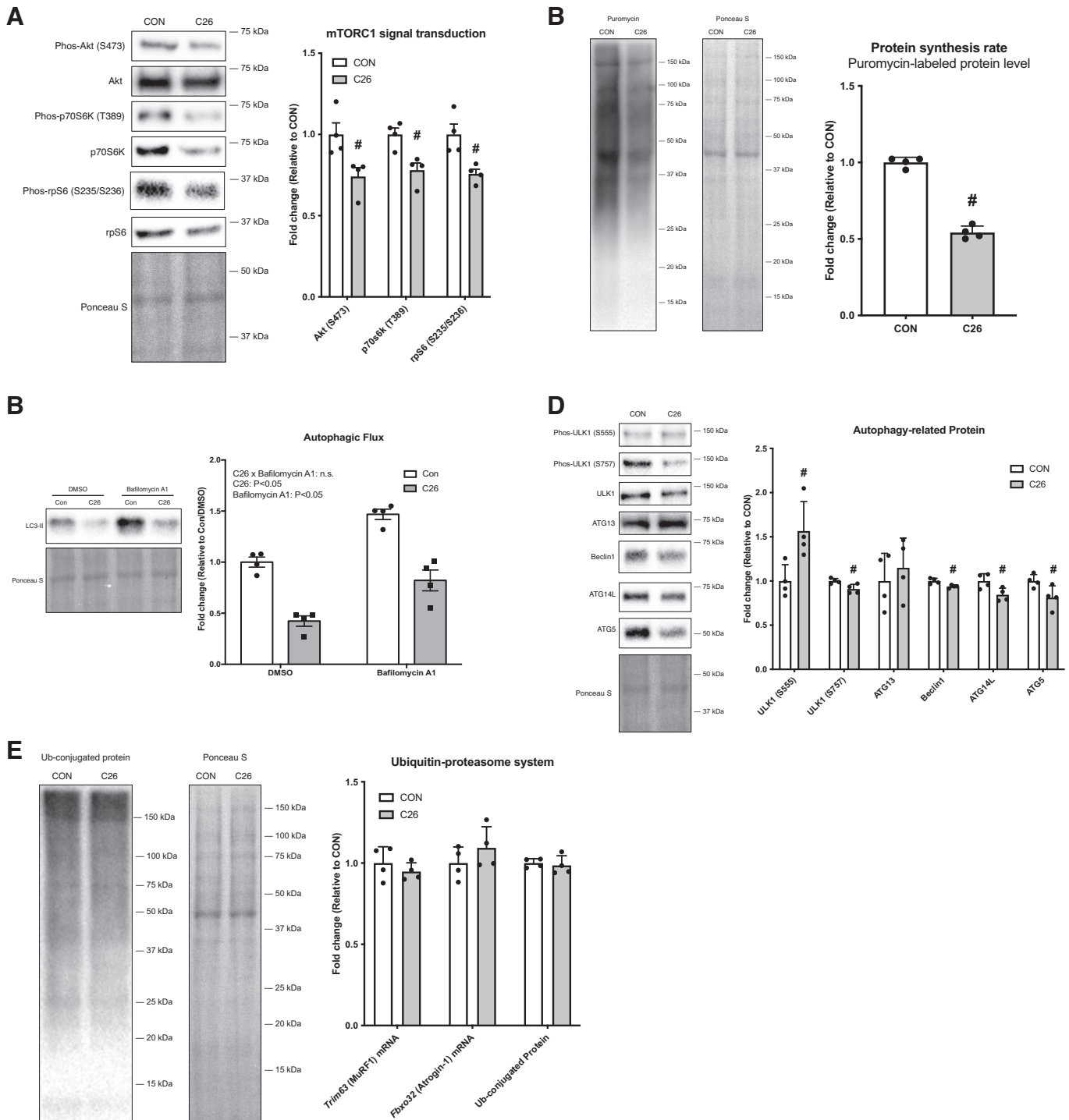


**Figure 3.** Coculture with Colon-26 cells attenuates mechanistic target of rapamycin complex 1 (mTORC1) signal transduction and the protein synthesis rate in C2C12 myotubes. **A:** information on the phosphorylated and total levels of proteins implicated in mTORC1 signal transduction. **B:** results of a puromycin incorporation-based assay used to assess the rate of protein synthesis. **C and D:** autophagic flux (C) and the levels of proteins involved in the induction of autophagy (D). **E:** both gene and protein expression levels of molecules associated with the ubiquitin-proteasome system. Notably, there is a significant difference ( $\#P < 0.05$  vs. CON) observed in the measured parameters. All data are presented as means  $\pm$  SD.

### Coculture with Colon-26 Cells Increases Glycolytic Enzyme Activity in C2C12 Myotubes

Next, we evaluated the activities of enzymes involved in glycolysis, such as hexokinase, glycogen phosphorylase, phos-

phofructokinase, and pyruvate kinase. These enzymes are irreversible and rate-limiting enzymes in glycolysis. Coculture with Colon-26 cells increased the activities of hexokinase, phosphofructokinase, and pyruvate kinase, but no effect was observed on glycogen phosphorylase activity (Fig. 5B).

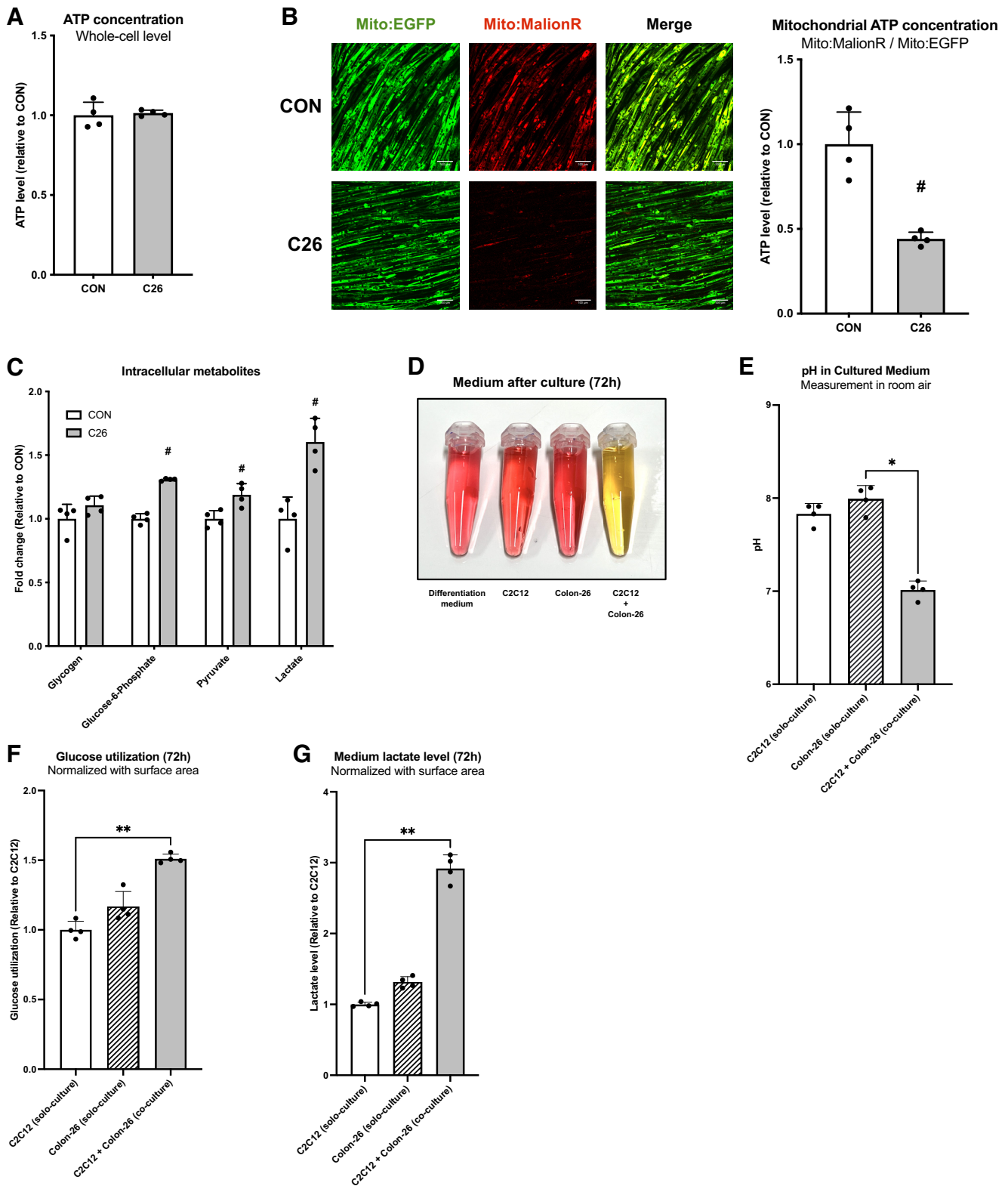


**Figure 4.** Coculture with Colon-26 cells increases glycolytic metabolites. **A:** concentration of ATP within the whole cell **B:** fluorescent biosensor-based assay is used to determine the concentration of ATP in mitochondria. EGFP, enhanced green fluorescent protein. **C:** data on intracellular metabolites associated with glycolysis. **D:** representative image of the culture medium used. **E:** pH of the culture medium. **F** and **G:** level of glucose utilization (**F**) and the concentration of lactate in the medium (**G**). Statistically significant differences are shown [# $P < 0.05$  vs. control (CON), \* $P < 0.05$  Colon-26 (solo-culture) vs. C2C12 + Colon-26 (co-culture), \*\* $P < 0.01$  C2C12 (solo-culture) vs. C2C12 + Colon-26 (co-culture)]. All data are presented as means  $\pm$  SD.

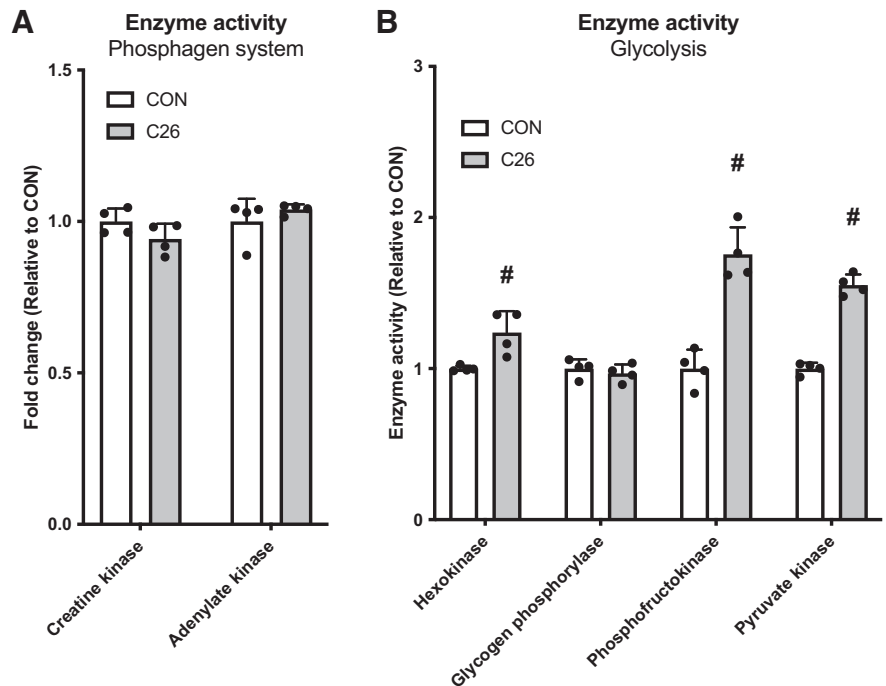


**Figure 5.** Coculture with Colon-26 cells increases glycolytic enzyme activity in C2C12 myotubes. *A*: data on the enzymatic activities associated with the phosphagen system. *B*: enzymatic activities implicated in glycolysis. Noteworthy differences are indicated [ $\#P < 0.05$  vs. control (CON)]. All data are presented as means  $\pm$  SD.

### Coculture with Colon-26 Cells Increases the Lactate Production Capacity in C2C12 Myotubes

We next evaluated adaptations related to pyruvate and lactate metabolisms. Lactate dehydrogenase (LDH) forms a tetramer composed of LDHA (a subunit with a high tendency to convert pyruvate to lactate) and/or LDHB (a subunit with a high tendency to convert lactate to pyruvate). Evaluation of LDH isozymes revealed that the proportion of LDH5 (A4) complexes, which have a high tendency to convert pyruvate to lactate, were increased by coculture with Colon-26 cells (Fig. 6A). Consistent with this result, lactate dehydrogenase activity (conversion of pyruvate into lactate) was significantly increased by coculture with Colon-26 cells (Fig. 6B). In terms of protein expression levels, LDHB expression did not change after coculture with Colon-26 cells, but LDHA expression was increased (Fig. 6C). Evaluation of the protein levels of MCT1 (high affinity/low transport capacity) and MCT4 (low affinity/high transport capacity), which are involved in lactate transport, revealed that the content of MCT1, but not MCT4, was increased by coculture with Colon-26 cells (Fig. 6C). These results suggested that coculture with Colon-26 cells induced adaptations to increase the capacity to convert pyruvate into lactate. In addition to conversion into lactate, pyruvate can also be oxidized as a substrate in mitochondria. Therefore, we evaluated adaptations of the initial steps involved in oxidation of pyruvate in mitochondria. Pyruvate produced in the cytosol is transported to the mitochondrial matrix by mitochondrial pyruvate carriers (MPCs) localized in the inner membrane of mitochondria, and subsequently converted to acetyl-CoA by the pyruvate dehydrogenase (PDH) complex. We therefore investigated whether coculture with Colon-26 cells induced adaptations in the expression levels of MPC1 and MPC2, the phosphorylation status of the regulatory domain of PDH (phosphorylation of PDH $\alpha$ 1 at Ser293), and PDH complex activity. However, no

significant changes were observed in any of these factors after coculture with Colon-26 cells (Fig. 6, D and E).

### Coculture with Colon-26 Cells Decreases Complex I-Driven Mitochondrial Respiration in C2C12 Myotubes

Next, we assayed the respiratory capacity of permeabilized myotubes. Under conditions of respiration coupled to ATP production (state 3) and basal respiration to maintain proton conductance (state 2), the following four sets of respiratory substrates were used: pyruvate + malate, glutamate + malate, octanoylcarnitine + malate, and succinate + rotenone (a complex I inhibitor to attenuate reverse electron flow). We found no significant effect of coculture with Colon-26 cells on state 2 respiration when any of the substrates were used (Fig. 7, A–D). However, under state 3 respiration, complex I-driven pyruvate + malate, glutamate + malate, and octanoylcarnitine + malate as substrates were significantly reduced by coculture with Colon-26 cells (Fig. 7, A–C). However, when complex II-driven succinate was used as the substrate, no negative effect of coculture with Colon-26 cells was observed (Fig. 7D).

To better understand the physiological basis underlying such adaptations of the mitochondrial respiratory function, we examined the effect of coculture with Colon-26 cells on enzymatic activity of the TCA cycle and respiratory chain of the electron transport chain. The enzymatic activities of citrate synthase, isocitrate dehydrogenase,  $\alpha$ -ketoglutarate dehydrogenase, succinate dehydrogenase (which is also complex II of the electron transport chain), and malate dehydrogenase were selected to measure the activities of TCA cycle enzymes. These enzymes are either irreversible or rate-limiting enzymes and supply NADH/FADH<sub>2</sub> to the electron transport chain. The activities of citrate synthase, isocitrate dehydrogenase, and  $\alpha$ -ketoglutarate dehydrogenase were decreased by Colon-26 cell coculture (Fig. 8A). However, no

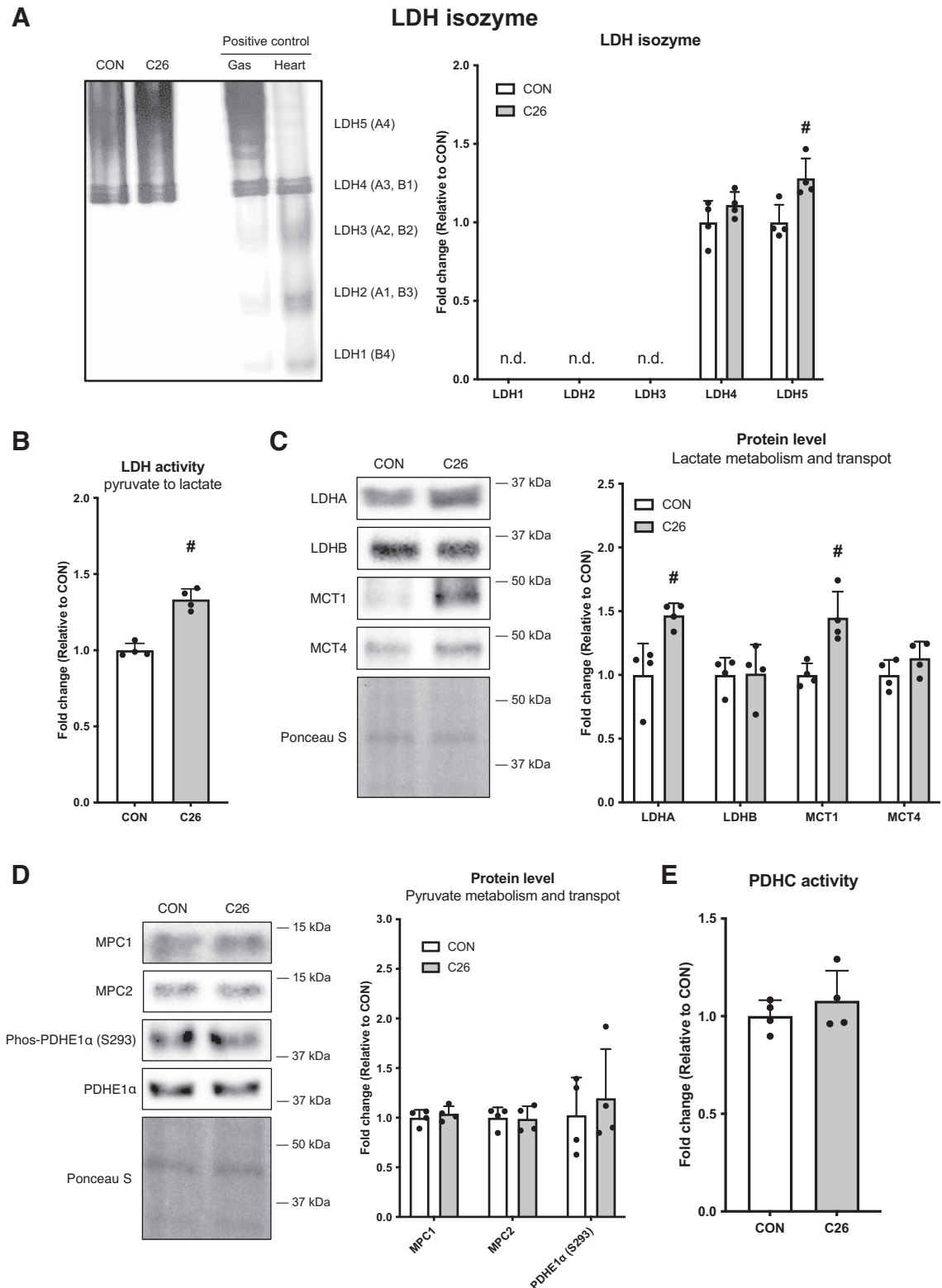


**Figure 6.** Coculture with Colon-26 cells increases the lactate production capacity in C2C12 myotubes. *A*: information on the lactate dehydrogenase (LDH) isozyme. *B*: measured enzyme activity of LDH. *C*: data on the concentration of proteins involved in lactate metabolism and transport. *D*: information on the levels of proteins implicated in pyruvate metabolism and transport. *E*: the enzymatic activity of pyruvate dehydrogenase complex (PDHC). Any significant differences are indicated [ $\#P < 0.05$  vs. control (CON)]. All data are presented as means  $\pm$  SD.

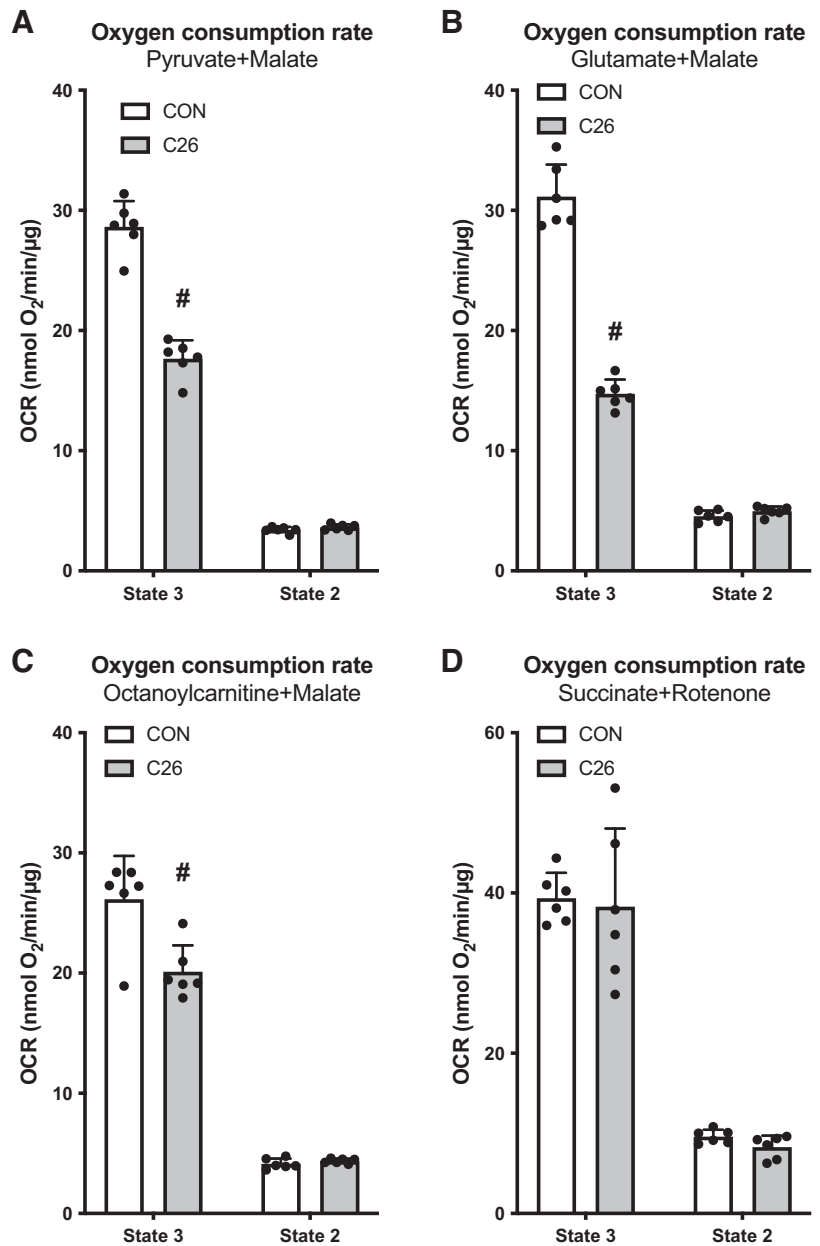


**Figure 7.** Coculture with Colon-26 cells decreases the complex I-driven mitochondrial oxygen consumption rate in C2C12 myotubes. *A*: oxygen consumption rate (OCR) when pyruvate and malate are used as substrates. *B*: oxygen consumption rate with glutamate and malate as substrates. *C*: oxygen consumption rate when octanoylcarnitine and malate serve as substrates. *D*: oxygen consumption rate using succinate and rotenone as substrates. Any significant differences are indicated [ $\#P < 0.05$  vs. control (CON)]. All data are presented as means  $\pm$  SD.

changes were observed in the activities of succinate or malate dehydrogenases (Fig. 8A). Next, we evaluated the enzymatic activity of the electron transport chain. Enzyme activity related to complex I (complex I and complex I + III) was decreased by coculture with Colon-26 cells (Fig. 8B). However, enzyme activity related to complex II (succinate dehydrogenase as shown above and complex II + III) was not affected by coculture with Colon-26 cells (Fig. 8, A and B). Recent studies have shown both the enzymatic activity of the respiratory chain alone and the status of the formation of large complexes (supercomplexes) among respiratory chains are important factors that affect the efficiency of the electron transport chain (47). Therefore, we evaluated the physical interactions among respiratory chains using two-dimensional electrophoresis. However, the supercomplex formed by respiratory chains I, III, and IV was not affected by coculture with Colon-26 cells (Fig. 8C).

We additionally evaluated whether the above-mentioned bioenergetic remodeling of mitochondria was associated with changes in mitochondrial integrity by assessing the membrane potential and superoxide production of mitochondria. As a result, coculture with Colon-26 cells increased the mitochondrial membrane potential (Fig. 9A) and mitochondrial superoxide levels (Fig. 9B). The decrease in the mitochondrial ATP production capacity can be attributed to the inability to dissipate the proton gradient in the mitochondrial intermembrane space and promotion of electron leakage from the electron transport chain. These adaptations are consistent with bioenergetic changes.

These findings suggested that adaptations of the mitochondrial respiratory capacity in response to coculture with Colon-26 cells were closely related to changes in enzymatic activity of the TCA cycle and electron transport chain.

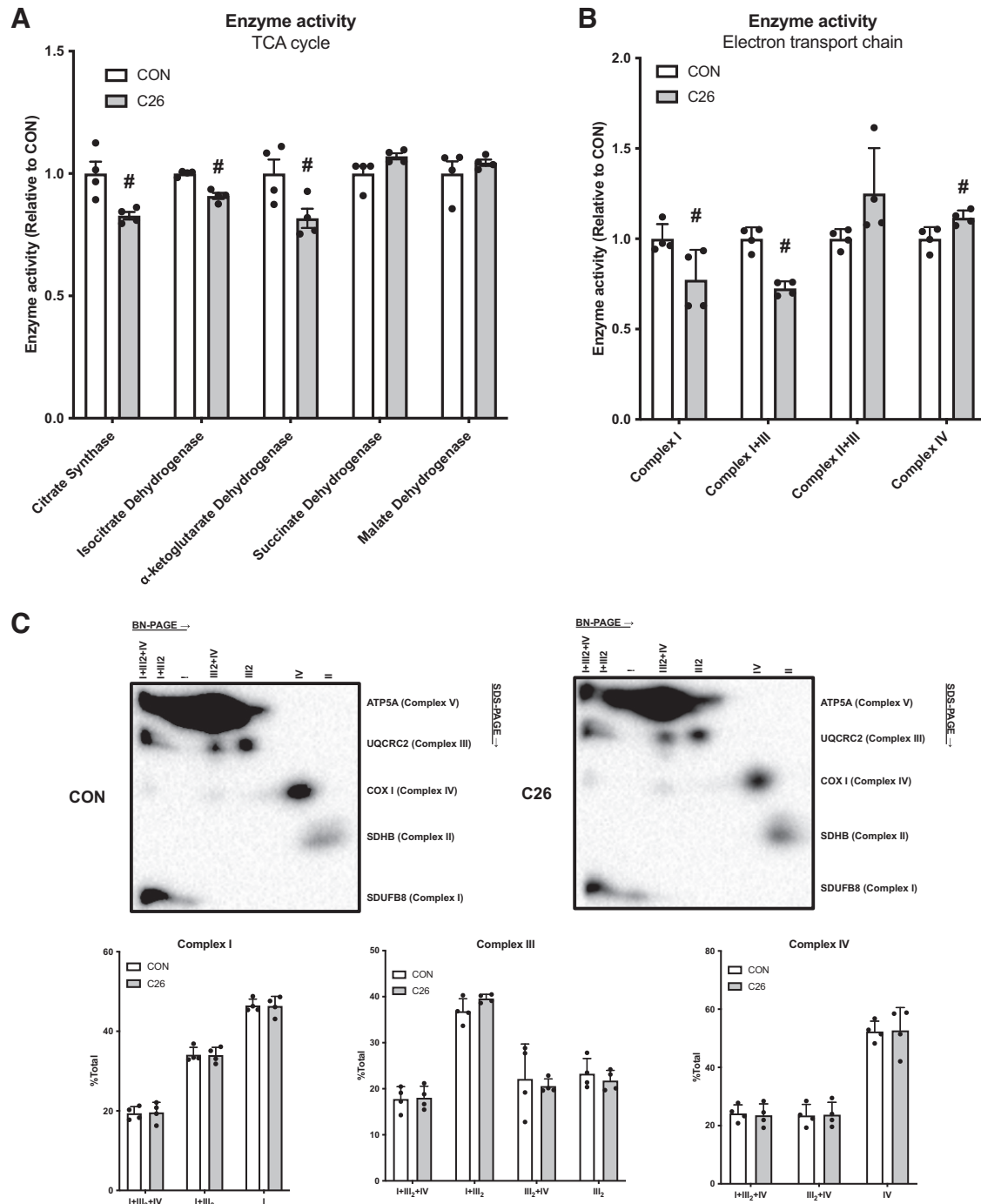


**Figure 8.** Coculture with Colon-26 cells partially decreases enzyme activity in the TCA cycle and electron transport chain in C2C12 myotubes. *A*: enzymatic activity related to the TCA cycle. *B*: enzymatic activity of the electron transport chain. *C*: results of the supercomplex assembly assay are presented. Statistically significant differences are indicated [ $\#P < 0.05$  vs. control (CON)]. All data are presented as means  $\pm$  SD.

### Coculture with Colon-26 Cells Does Not Drive the Adaptive Mitochondrial Quality Control Response in C2C12 Myotubes

We subsequently investigated whether the functional and qualitative changes in mitochondria were accompanied by adaptations in mitochondrial quality control machinery. Mitochondrial homeostasis is maintained by quality control systems at molecular and organelle levels. At the molecular

level, molecular chaperones and proteases play a role, which is referred to as the mitochondrial unfolded protein response. In the context of mitochondrion-localized molecular chaperones, coculture with Colon-26 cells had no apparent effect on mtHSP70 or TRAP1 proteins but decreased expression of HSP60 (Fig. 10A). Coculture with Colon-26 cells also reduced the levels of the mitochondrion-localized proteases CLPP and Omi/HtrA2 (Fig. 10A). These results suggested that coculture with Colon-26 cells reduced the expression of

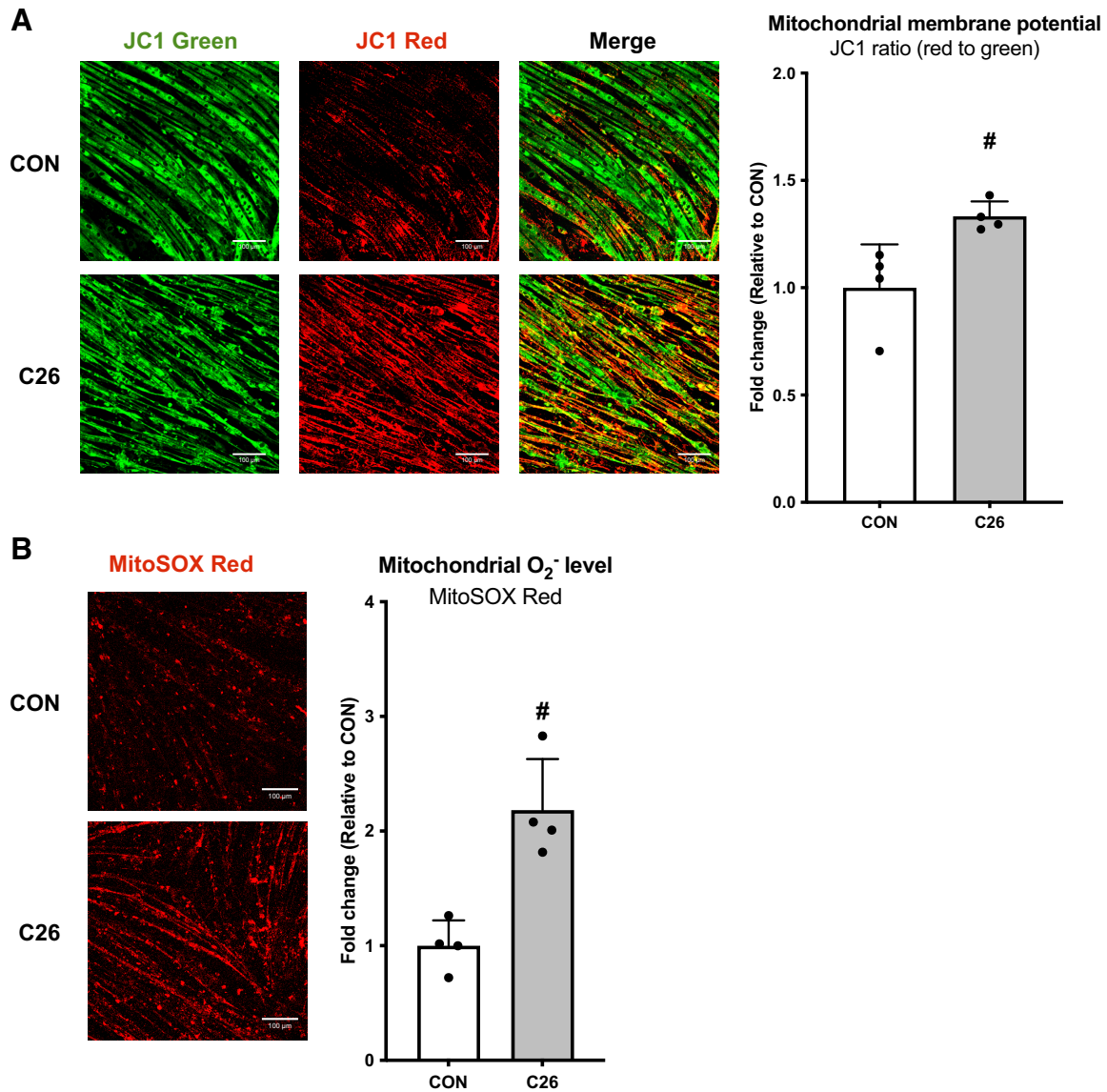


**Figure 9.** Coculture with Colon-26 cells increases the mitochondrial membrane potential and superoxide in C2C12 myotubes *A*: data from a JC1-based assay used to evaluate the mitochondrial membrane potential. *B*: mitochondrial superoxide level, as determined by the MitoSOX Red-based assay. Any statistically significant differences are indicated [ $\#P < 0.05$  vs. control (CON)]. All data are presented as means  $\pm$  SD.

some mitochondrial chaperones and proteases and thus reduced mitochondrial quality control capabilities at the molecular level. To further assess quality control at the mitochondrial organelle level, we examined proteins that regulate mitochondrial morphology and dynamics. We found that the contents of fusion-regulating proteins MFN2 and OPA1 (active form: L-OPA1; inactive form: S-OPA1; active status: L-OPA1/S-OPA1) and the fission-regulating protein DRP1 were reduced by coculture with Colon-26 cells (Fig. 10B). However, upon qualitatively evaluating mitochondrial morphology in myotubes, no significant effects were observed (Fig. 10C).

#### Coculture with Colon-26 Cells Decreases Expression of Genes Involved in Muscle Development but Increases Expression of a Series of Genes Involved in Glycolysis

We wanted to determine the extent to which the molecular physiological responses and adaptations to coculture

with Colon-26 cells were consistent with the changes in the transcript levels. Therefore, we performed gene expression profiling by RNA-seq and bioinformatics analysis. An overview of genes with altered expression is shown in a volcano plot (Fig. 11A). There were 427 upregulated genes and 119 downregulated genes (false discovery rate cutoff: 0.10, minimal fold change: 2) in coculture with Colon-26 cells. The top 15 upregulated and top 15 downregulated genes are shown in Fig. 11, B and C. We conducted pathway analyses of genes with significantly changed expression by referring to GO, KEGG, and Reactome databases. Notable results showed that pathways related to skeletal muscle structure development were predicted to be inactivated by the GO database as a reference (Fig. 12, A and B). Furthermore, when KEGG (Fig. 12, A and C) and Reactome (Fig. 12, A and D) databases were used as references, pathways related to glycolysis were predicted to be activated. These results were highly consistent

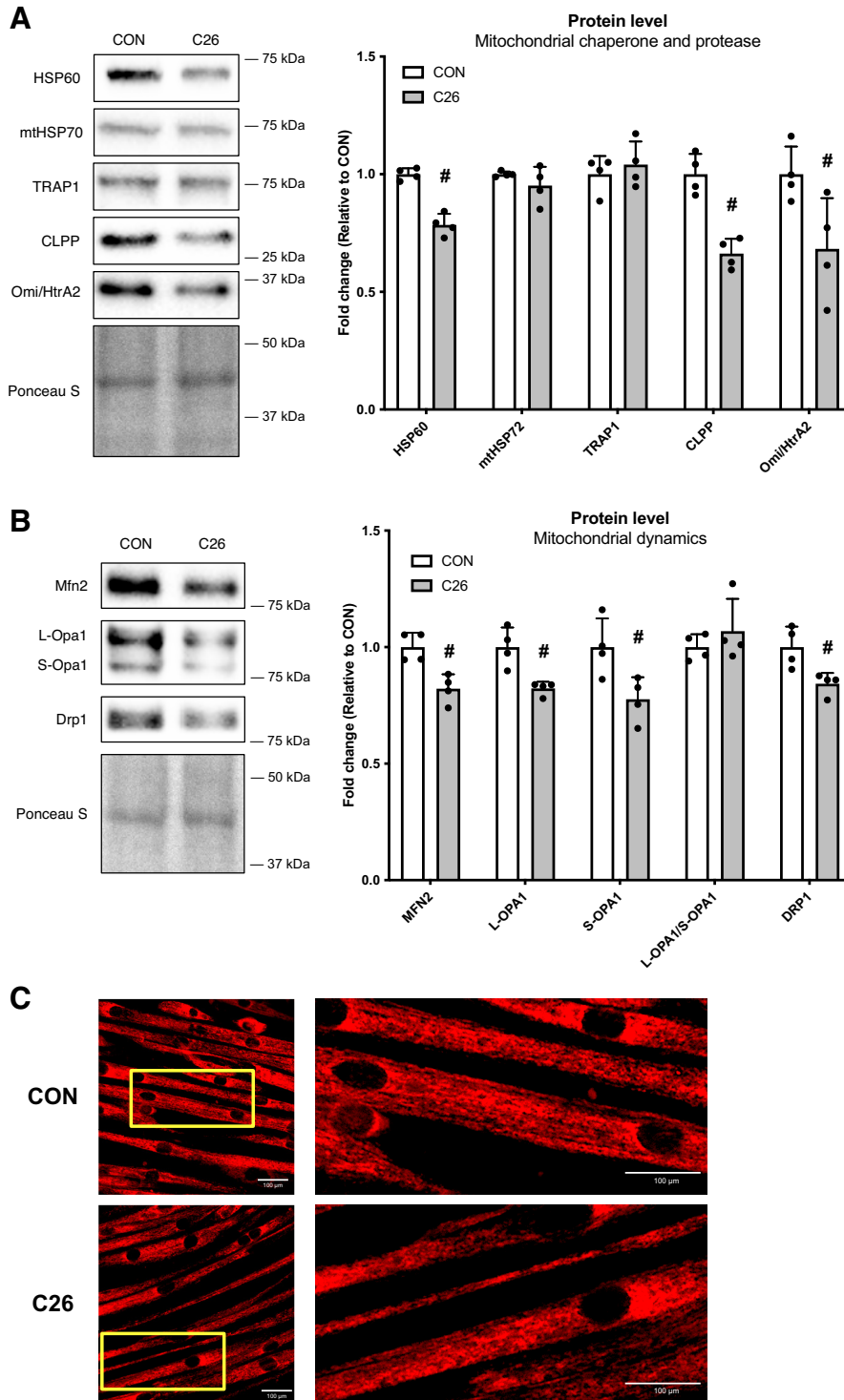


**Figure 10.** Coculture with Colon-26 cells partially decreases the levels of protein involved in mitochondrial quality control in C2C12 myotubes. *A*: protein levels of mitochondrial chaperones and proteases. *B*: data on the levels of proteins that regulate mitochondrial dynamics. *C*: representative images to highlight the changes in mitochondrial morphology. Statistically significant differences are indicated [ $\#P < 0.05$  vs. control (CON)]. All data are presented as means  $\pm$  SD.

with atrophy of myotubes and enhancement of the glycolysis pathway upon coculture with Colon-26 cells. However, coculture with Colon-26 cells reduced mitochondrial oxidative metabolism (complex I driven) but did not result in a marked reduction in expression of mitochondrion-related genes or enrichment of pathways involved in oxidative energy metabolism in the inactivated pathways. Complete data related to gene expression profiling and bioinformatics

are provided in Supplemental Data S1 (<https://doi.org/10.6084/m9.figshare.22723243.v1>).

#### Effect of Coculture with Primary Epithelial Cells of Colon Origin on C2C12 Myotubes

Possible concerns were raised about whether the adaptations observed in C2C12 myotubes when cocultured with Colon-26 cells stemmed solely from the interaction with a

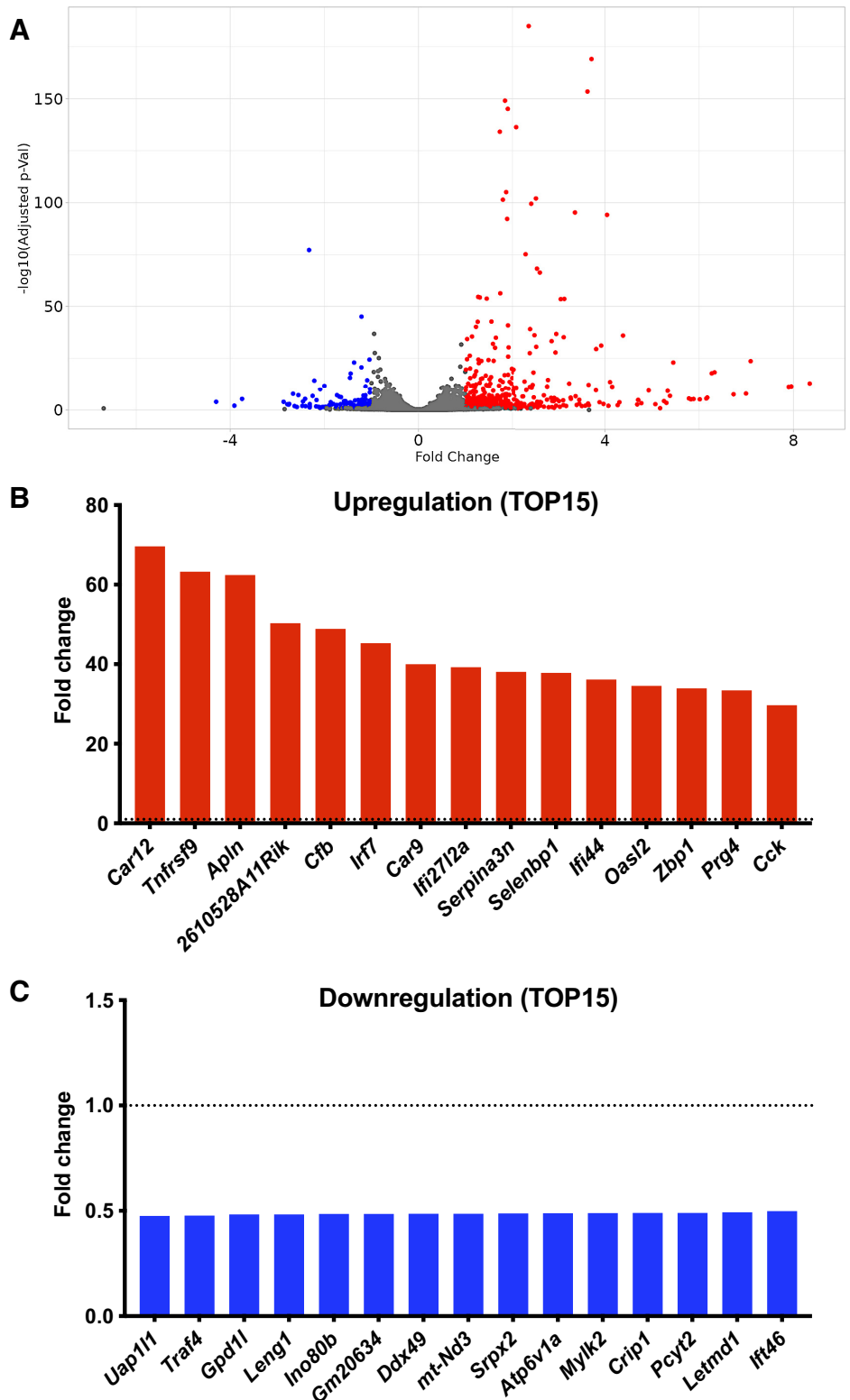


**Figure 11.** Gene expression profiling of C2C12 myotubes after coculture with Colon-26 cells. *A*: volcano plot highlighting the significance and magnitude of changes in gene expression. *B* and *C*: top 15 significantly upregulated genes (*B*) and the top 15 significantly downregulated genes (*C*).

different cell type or were attributable to variations in cell culture density. To address these possible concerns, a follow-up experiment was conducted. Primary epithelial cells, isolated from the mouse colon and exhibiting over 95% purity as evidenced by cytokeratin 18 positivity (Supplemental Fig. S5A), were cocultured with C2C12 myotubes. This

approach aimed to assess the specificity of the adaptations observed above. The selection of parameters for measurement was informed by those changes noted in C2C12 myotubes cocultured with Colon-26 cells (Supplemental Figs. S5–S7). The findings demonstrated that most measured parameters did not show significant adaptations in C2C12 myotubes

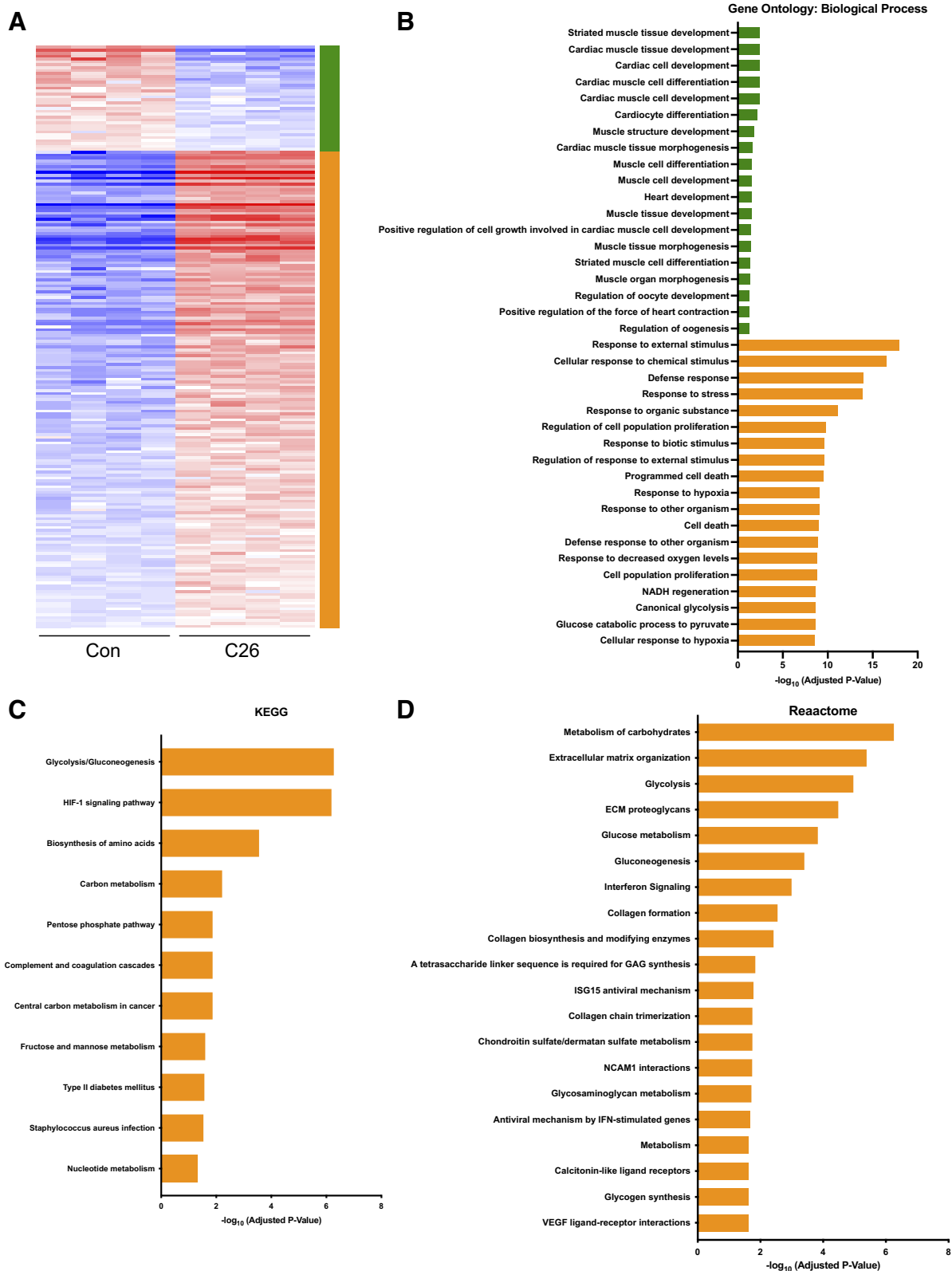


**Figure 12.** Pathway analysis of significantly altered gene expression. *A*: cluster analysis of significantly changed gene expression *B*: pathway enrichment analysis by Gene Ontology biological processes. *C*: pathway enrichment analysis conducted using the Kyoto Encyclopedia of Genes and Genomes (KEGG). *D*: pathway enrichment analysis completed using Reactome. ECM, extracellular matrix.

when cocultured with primary epithelial cells. A notable exception was the observed decrease in mitochondrial superoxide levels in C2C12 myotubes cocultured with primary epithelial cells (Supplemental Fig. S7B), contrasting with the increase in superoxide levels noted when cocultured with Colon-26 cells (Fig. 9B). This distinct response indicates a specific adaptation to coculture conditions rather than a general response to cell density or cell type variance. In summary, the adaptations induced in C2C12 myotubes by coculture with Colon-26 cells are 1) not merely the consequence of coculturing with a different cell type, 2) not solely attributable to variations in the number of cultured cells, and 3) specifically related to interactions with cancerous colon-derived epithelial cells, distinguishing these effects from those observed with primary colon-derived epithelial cells.

## DISCUSSION

### Protein Synthesis and Degradation Mechanisms

In an *in vivo* Colon-26-xenografted model, inactivation of the mTORC1 pathway, a subsequent decrease in protein synthesis, and activation of the proteolysis system are observed (48, 49). However, in the coculture model of Colon-26 cells and C2C12 myotubes in this study, inactivation of protein synthesis pathways centered on mTORC1 was similarly observed to the *in vivo* model, but activation of protein degradation pathways (i.e., autophagy-lysosome and ubiquitin-proteasome systems) was not observed. These results indicate that atrophy of myotubes due to coculture with Colon-26 cells can be mainly explained by a decrease in the protein synthesis capacity. Therefore, the enhancement of protein degradation in skeletal muscle observed in Colon-26 tumor-bearing mice may not be a direct result of the interaction between cancer cells/tumors and skeletal muscles but may be triggered by other cell types, organs, or behavioral changes. For example, the Colon-26-xenografted mouse model exhibits increases in various cytokines (e.g., TNF- $\alpha$  and IL-6) in circulation (50). These cytokines provide sufficient stimulation to cause muscle atrophy (51). Furthermore, analyses using blocking antibodies or knockout animal models have shown that the increase in concentrations of these cytokines is necessary for cancer-induced skeletal muscle atrophy (52, 53). Mechanistically, these cytokines activate the transcription factor FoxO family and transcriptional control processes of the ubiquitin-proteasome and autophagy-lysosome systems (54–56). Importantly, a previous study of conditioned medium from Colon-26 cells has shown that Colon-26 cells themselves do not secrete at least TNF- $\alpha$  or IL-6 (57). Therefore, possible interpretations of the increase in these cytokines in the *in vivo* model are increased secretion from cells other than Colon-26 or Colon-26 becoming secretory as a result of interactions with other cell types. Moreover, cancer cachexia decreases food intake and physical activity, leading to muscle disuse (8). Decreases in food intake and physical activity are well accepted as sufficient stimuli to activate autophagy-lysosome and ubiquitin-proteasome system (58, 59). Furthermore, interestingly, our gene expression profiling and pathway analysis (GO biological processes) by RNA-seq suggested inactivation of multiple pathways related to skeletal muscle formation. Evaluation of the proteins of these

differentially expressed genes was not performed in this study, but it is possible that skeletal muscle atrophy may also have progressed because of a decrease or dysfunction of the molecules responsible for skeletal muscle formation and maintenance, in addition to the balance of protein synthesis and degradation.

### Glycolytic Energy Metabolism

Changes in energy metabolism due to cancer cachexia have been considered simply to be a result of the condition. However, in recent years, these changes in energy metabolism have been suggested to be a possible cause or exacerbating factor of cancer cachexia and even a potential therapeutic target (15, 16). In coculture with Colon-26 cells, the intracellular ATP concentration was unexpectedly maintained at a constant level. However, the ATP level in mitochondria was decreased, and compensatory activation of glycolytic metabolism was demonstrated by increased glycolytic metabolites and enzymatic activity. When mitochondrial ATP synthesis is impaired, the intracellular ADP/ATP ratio is known to increase (60). This elevation in cellular ADP/ATP activates rate-limiting enzymes (such as PFK) involved in glycolysis, thereby inducing a compensatory shift in ATP source (60). This metabolic adjustment has been observed both in model cells derived from patients with mitochondrial diseases and experimentally in cells treated with Oligomycin, a recognized inhibitor of mitochondrial ATP synthase (60, 61). The observed shift in energy metabolism when cocultured with Colon-26 cells in this study may be indicative of a similar adaptive mechanism. In a mouse model, adaptation of glycolysis to cancer cachexia has not received as much attention as mitochondrial oxidative energy production. Visavadiya et al. (62) recently reported increases in the lactate-to-pyruvate ratio, LDH activity, and MCT1 protein in a mouse-bearing Colon-26 tumor. Although enzymatic activity of glycolysis was not reported in the study, it was suggested that glycolysis was activated during cancer cachexia progression. If we assume that glycolysis was also activated in our cocultures and mouse cachexia models, glycolysis activation in skeletal muscle by cancer cachexia indicates that it can be at least partly explained by direct interactions between cancer cells and skeletal muscle cells. Gene expression profiling and pathway analyses (KEGG and Reactome) of RNA-seq data in this study revealed the top pathways expected to activate the glycolytic pathway. These results indicate that glycolysis activation by coculture matches well with the changes at the transcriptional level. Therefore, evaluation at the transcriptional level may be useful to understand the mechanisms by which glycolysis is activated by coculture or cachexia. For example, transcription factors, such as HIF-1 and c-Myc, are promising candidates for common transcriptional factors driving gene transcription involved in glycolytic enzymes (63).

### Mitochondrial Oxidative Metabolism

A decrease in mitochondrial oxidative energy metabolism has been recently reported in cancer cachexia by various studies. In this study, ATP levels in mitochondria were decreased by coculture with Colon-26 cells. To clarify the physiological background of these findings, we revealed the

metabolic mechanisms of mitochondria through an element reduction approach. We observed that the respiratory capacity coupled to ATP production in mitochondria was dependent on the substrate. While the respiratory capacity through pathways involving complex I was decreased, complex II was unaffected by coculture. In an *in vivo* cachexia model, changes in the mitochondrial respiratory capacity using succinate as a substrate were mild compared with pyruvate and malate (18). Therefore, the changes in the mitochondrial respiratory capacity observed in the *in vivo* cachexia model may be partially explained by the direct interactions between cancer cells and skeletal muscle cells.

Functional evaluation of mitochondria yields various interpretations depending on evaluation of isolated mitochondria or permeabilized cells. This study investigated the mitochondrial oxidative capacity in permeabilized myotubes, which reflects changes in mitochondrial content and the oxidative capacity per unit mitochondrion and changes in factors other than mitochondria that may affect mitochondrial respiration. As part of the evaluation of TCA enzyme activity, we measured CS activity, which is a marker of mitochondrial content. However, other biomarkers for mitochondrial content, such as the protein level of subunits comprising the respiratory chain complex or the copy number of mitochondrial DNA, do not necessarily correlate with changes in CS activity (Supplemental Fig. S8, A and B). Moreover, the expression level of peroxisome proliferator-activated receptor- $\gamma$  coactivator-1 $\alpha$  (PGC-1 $\alpha$ ), a master regulator of mitochondrial biogenesis, did not change in coculture (Supplemental Fig. S8C). Integrating these results suggested that the quantitative changes in mitochondria induced by coculture were either minimal or nonexistent. Therefore, the decrease in the mitochondrial oxygen consumption rate and enzyme activities related to complex I in the TCA cycle and the electron transport chain reflected a functional decline per unit mitochondrion rather than a decrease in mitochondrial content. Conversely, previous studies in mice (17, 20, 64) have reported that transplantation of Colon-26 cells decreases the protein contents of respiratory chain complex subunits, suggesting that, both functional and quantitative changes in mitochondria occur in the skeletal muscle of the Colon-26 xenografted model. Notably, a recent study by Delfinis and colleagues (17) found a reduction in the mitochondrial respiratory capacity in permeabilized skeletal muscle, but the functional changes were retained even when corrected for the expression level of electron transport chain subunits. Therefore, both functional and quantitative changes in mitochondria are evident *in vivo*, but in our coculture model, functional changes were predominant. Thus the loss of mitochondrial function due to cancer cachexia can be explained, at least in part, by direct interactions between Colon-26 cells and skeletal muscle cells, while quantitative changes in mitochondrial content are induced by other factors such as other organs, other cell types, or behavioral changes.

Mitochondrion-related genes were not significantly downregulated in the gene expression analysis by RNA-seq, and they were not enriched in pathways that were predicted to be inactivated. A possible explanation for adaptations such as the decreased ATP production capacity of mitochondria in coculture is that changes in posttranscriptional or translational

processes, rather than transcription-level changes, are the main contributing factors. Our results indicated that coculture with Colon-26 caused a decline in global protein synthesis, reduced autophagic activity, and decreased mitochondrial chaperones and proteases. These observations suggest a compromise in the mitochondrial capacity for protein turnover and quality control. However, when referring to RNA-seq data from skeletal muscle in an *in vivo* cancer cachexia model, mitochondrial dysfunctions were supported by changes in transcriptional levels (65). Therefore, in the mouse model of cachexia, changes in behavior and/or humoral factors from other organs and cell types to skeletal muscle may also modulate both mitochondrial functions and contents at the transcriptional level. This idea is supported by the finding that the *in vivo* content of PGC-1 $\alpha$ , a strong transcriptional driver of mitochondrion-related genes, is reduced in skeletal muscle by Colon-26 cells (64), whereas no change was observed in PGC-1 $\alpha$  content in the coculture model of this study (Supplemental Fig. S8C).

### Bidirectional Communication between Colon-26 Cells and C2C12 Myotubes

We performed noncontact coculture using cell culture inserts with a pore size of 1  $\mu\text{m}$ . Therefore, intercellular communication between cells was mediated by soluble proteins, miRNAs, metabolites, and nonsoluble factors with a size of 1  $\mu\text{m}$  or less, such as extracellular vesicles. In a study using conditioned medium from Colon-26 cells, it was reported that leukemia inhibitory factor (LIF) derived from Colon-26 cells was the main factor inducing atrophy of myotubes (57). To the best of our knowledge, no reports have examined whether LIF also remodels energy metabolism. We cannot conclude whether myotube atrophy and metabolic remodeling toward glycolysis dominance were induced by a single factor such as LIF or other contributing factors. If a factor inducing a shift glycolysis metabolism can be identified, the development of new therapies may be possible using neutralizing antibodies or receptor inhibitors of such a factor.

To clarify the metabolic adaptations of C2C12 myotubes, we also examined some metabolic adaptations in Colon-26 cells cocultured with C2C12 myotubes. The results showed that coculture with C2C12 myotubes enhanced the mitochondrial respiratory capacity when pyruvate + malate and succinate were used as substrates. These metabolic adaptations may affect the proliferative capacity of Colon-26 cells and the secretory kinetics of cachexic humoral factors. Because this study focused specifically on skeletal muscle adaptations, the adaptations of Colon-26 cells during coculture were not sufficiently examined. Skeletal muscle cells secrete myokines and extracellular vesicles (66). *In vivo* cancer cachexia models have shown that exercise and skeletal muscle contraction are effective in improving various symptoms of cachexia (67). Therefore, a future research direction may be to evaluate the adaptation of Colon-26 cells when experimentally manipulating C2C12 myotubes cocultured with Colon-26 cells, such as electrical stimulation-induced contraction. By conducting such studies, new evidence supporting the effectiveness of exercise therapy for cancer cachexia may be obtained.

## Advantages and Limitations of Coculture as an In Vitro Cachexia Model

Even though it is crucial to consider the differences between skeletal muscle fibers in vivo and myotubes in vitro, in vitro experimental models have established their value in various domains. These include drug treatments, genetic manipulation, imaging, and the elucidation of mechanisms. Despite the inherent limitations, their utility remains significant in the progression of research. Recently, there has been a growing demand to replace in vivo experiments with in vitro models as much as possible from an animal welfare standpoint. This is particularly relevant to cancer cachexia, and coculturing Colon-26 cells and C2C12 myotubes has been used in several studies as an in vitro cachexia model. However, the previous studies were based on limited knowledge, such as a decrease in the myotube diameter (11). As discussed in this study, we organized the potential adaptations that can and cannot be explained by direct cross talk between cancer cells and skeletal muscle cells in the pathophysiology of cancer cachexia in vivo. Our findings suggest that it is important to consider whether the experimental purpose and model characteristics are aligned when using coculture as an in vitro cachexia model. For example, it may be useful to screen drugs that attenuate Colon-26 cell-induced inhibition of the mTORC1 pathway and protein synthesis in skeletal muscle cells due to cachexia. However, it may not be suitable to search for potential drugs that suppress upregulation of protein breakdown in skeletal muscles due to cachexia, because the protein degradation mechanism, especially ubiquitin-proteasome and autophagy-lysosomal systems, is not activated in a coculture model with Colon-26 cells.

## Conclusions

We investigated the adaptation of skeletal muscle cells through potential direct cross talk with cancer cells by conducting noncontact coculture of Colon-26 cells and C2C12 myotubes to further understand the complex pathological condition of cancer cachexia. Protein synthesis machinery in C2C12 myotubes was markedly inhibited and myotube atrophy occurred in coculture with Colon-26 cells. Furthermore, energy metabolism in C2C12 myotubes was significantly shifted toward glycolytic energy metabolism rather than oxidative energy metabolism in coculture. The increased activity of glycolytic enzymes was consistent with gene expression levels, but the decreased ATP production capacity in mitochondria was not consistent with the changes in gene expression. The findings of direct interactions between cancer cells and skeletal muscle cells obtained in this study may contribute to a more fundamental understanding of the complex pathophysiology of cancer cachexia.

## DATA AVAILABILITY

The data that support the findings of this study are available in the main text and/or supplemental material of this article.

## SUPPLEMENTAL DATA

Supplemental Document S1: <https://doi.org/10.6084/m9.figshare.23574279.v1>.

Supplemental Figs. S1–S8: <https://doi.org/10.6084/m9.figshare.25426069.v3>.

Supplemental Tables S1 and S2: <https://doi.org/10.6084/m9.figshare.23574276.v1>.

Supplemental Data S1: <https://doi.org/10.6084/m9.figshare.22723243.v1>.

## GRANTS

Funding was provided by a Nippon Sport Science University Research Grant (to Y. Tamura), Japan Society for the Promotion of Science (JSPS) Grant-in-Aid for Scientific Research (B) (21H03332 to Y. Tamura), and JSPS Grant-in-Aid for Challenging Research (20K21771 and 23K17452 to Y. Tamura).

## DISCLOSURES

No conflicts of interest, financial or otherwise, are declared by the authors.

## AUTHOR CONTRIBUTIONS

Y.T. conceived and designed research; Y.T. performed experiments; Y.T. analyzed data; Y.T., K.K., T.K., and K.N. interpreted results of experiments; Y.T. prepared figures; Y.T. drafted manuscript; Y.T., K.K., T.K., and K.N. edited and revised manuscript; Y.T., K.K., T.K., and K.N. approved final version of manuscript.

## REFERENCES

1. Fearon K, Strasser F, Anker SD, Bosaeus I, Bruera E, Fainsinger RL, Jatoi A, Loprinzi C, MacDonald N, Mantovani G, Davis M, Muscaritoli M, Ottery F, Radbruch L, Ravasco P, Walsh D, Wilcock A, Kaasa S, Baracos VE. Definition and classification of cancer cachexia: an international consensus. *Lancet Oncol* 12: 489–495, 2011. doi:10.1016/S1470-2045(10)70218-7.
2. Tan BH, Fearon KC. Cachexia: prevalence and impact in medicine. *Curr Opin Clin Nutr Metab Care* 11: 400–407, 2008. doi:10.1097/MCO.0b013e328300ecc1.
3. Kasvis P, Viganò M, Viganò A. Health-related quality of life across cancer cachexia stages. *Ann Palliat Med* 8: 33–42, 2019. doi:10.21037/apm.2018.08.04.
4. Baracos VE, Mazurak VC, Bhullar AS. Cancer cachexia is defined by an ongoing loss of skeletal muscle mass. *Ann Palliat Med* 8: 3–12, 2019. doi:10.21037/apm.2018.12.01.
5. Dewys WD, Begg C, Lavin PT, Band PR, Bennett JM, Bertino JR, Cohen MH, Douglass HO, Engstrom PF, Ezdinli EZ, Horton J, Johnson GJ, Moertel CG, Oken MM, Perlia C, Rosenbaum C, Silverstein MN, Skeel RT, Sponzo RW, Tormey DC. Prognostic effect of weight loss prior to chemotherapy in cancer patients. *Am J Med* 69: 491–497, 1980. doi:10.1016/S0149-2918(05)80001-3.
6. Rausch V, Sala V, Penna F, Porporato PE, Ghigo A. Understanding the common mechanisms of heart and skeletal muscle wasting in cancer cachexia. *Oncogenesis* 10: 1, 2021. doi:10.1038/s41389-020-00288-6.
7. Porporato PE. Understanding cachexia as a cancer metabolism syndrome. *Oncogenesis* 5: e200–e200, 2016. doi:10.1038/oncsis.2016.3.
8. Villars F, Pietra C, Giuliano C, Lutz T, Riediger T. Oral treatment with the ghrelin receptor agonist hm01 attenuates cachexia in mice bearing colon-26 (C26) tumors. *Int J Mol Sci* 18: 986, 2017. doi:10.3390/ijms18050986.
9. Halle JL, Counts-Franch BR, Prince RM, Carson JA. The effect of mechanical stretch on myotube growth suppression by colon-26 tumor-derived factors. *Front Cell Dev Biol* 9: 690452, 2021. doi:10.3389/fcell.2021.690452.
10. Silva KA, Dong J, Dong Y, Dong Y, Schor N, Tweardy DJ, Zhang L, Mitch WE. Inhibition of Stat3 activation suppresses caspase-3 and the ubiquitin-proteasome system, leading to preservation of muscle

- mass in cancer cachexia. *J Biol Chem* 290: 11177–11187, 2015. doi:10.1074/jbc.M115.641514.
11. **Jackman RW, Floro J, Yoshimine R, Zitin B, Eiamplikul M, El-Jack K, Seto DN, Kandarian SC.** Continuous release of tumor-derived factors improves the modeling of cachexia in muscle cell culture. *Front Physiol* 8: 738, 2017 [Erratum in *Front Physiol* 10: 394, 2019]. doi:10.3389/fphys.2017.00738.
  12. **Lautaoja JH, Pekkala S, Pasternack A, Laitinen M, Ritvos O, Hulmi JJ.** Differentiation of murine C2C12 myoblasts strongly reduces the effects of myostatin on intracellular signaling. *Biomolecules* 10: 695, 2020. doi:10.3390/biom10050695.
  13. **Li W, Trieu J, Blazev R, Parker BL, Murphy KT, Swiderski K, Lynch GS.** Sulforaphane attenuates cancer cell-induced atrophy of C2C12 myotubes. *Am J Physiol Cell Physiol* 324: C205–C221, 2023. doi:10.1152/ajpcell.00025.2022.
  14. **Murphy KT, Hossain MI, Swiderski K, Chee A, Naim T, Trieu J, Haynes V, Read SJ, Stapleton DI, Judge SM, Trevino JG, Judge AR, Lynch GS.** Mas receptor activation slows tumor growth and attenuates muscle wasting in cancer. *Cancer Res* 79: 706–719, 2019. doi:10.1158/0008-5472.CAN-18-1207.
  15. **Rohm M, Zeigerer A, Machado J, Herzig S.** Energy metabolism in cachexia. *EMBO Rep* 20: e47258, 2019. doi:10.15252/embr.201847258.
  16. **Fearon KC, Glass DJ, Guttridge DC.** Cancer cachexia: mediators, signaling, and metabolic pathways. *Cell Metab* 16: 153–166, 2012. doi:10.1016/j.cmet.2012.06.011.
  17. **Delfinis LJ, Bellissimo CA, Gandhi S, DiBenedetto SN, Garibotti MC, Thuhan AK, Tsitkanou S, Rosa-Caldwell ME, Rahman FA, Cheng AJ, Wiggs MP, Schlattner U, Quadraltero J, Greene NP, Perry CG.** Muscle weakness precedes atrophy during cancer cachexia and is linked to muscle-specific mitochondrial stress. *JCI Insight* 7: e155147, 2022. doi:10.1172/jci.insight.155147.
  18. **Halle JL, Pena GS, Paez HG, Castro AJ, Rossiter HB, Visavadiya NP, Whitehurst MA, Khamoui AV.** Tissue-specific dysregulation of mitochondrial respiratory capacity and coupling control in colon-26 tumor-induced cachexia. *Am J Physiol Regul Integr Comp Physiol* 317: R68–R82, 2019. doi:10.1152/ajpregu.00028.2019.
  19. **White JP, Baltgalvis KA, Puppa MJ, Sato S, Baynes JW, Carson JA.** Muscle oxidative capacity during IL-6-dependent cancer cachexia. *Am J Physiol Regul Integr Comp Physiol* 300: R201–R211, 2011. doi:10.1152/ajpregu.00300.2010.
  20. **Neyroud D, Nosacka RL, Judge AR, Hepple RT.** Colon 26 adenocarcinoma (C26)-induced cancer cachexia impairs skeletal muscle mitochondrial function and content. *J Muscle Res Cell Motil* 40: 59–65, 2019. doi:10.1007/s10974-019-09510-4.
  21. **Pin F, Huot JR, Bonetto A.** The mitochondria-targeting agent mitoch improves muscle atrophy, weakness and oxidative metabolism in C26 tumor-bearing mice. *Front Cell Dev Biol* 10: 861622, 2022. doi:10.3389/fcell.2022.861622.
  22. **Whitehead RH, Robinson PS.** Establishment of conditionally immortalized epithelial cell lines from the intestinal tissue of adult normal and transgenic mice. *Am J Physiol Gastrointest Liver Physiol* 296: G455–G460, 2009. doi:10.1152/ajpgi.90381.2008.
  23. **Uno H, Kamiya S, Akimoto R, Hosoki K, Tadano S, Kouzaki K, Tamura Y, Kotani T, Isemura M, Nakazato K.** Low-frequency electrical stimulation of bilateral hind legs by belt electrodes is effective for preventing denervation-induced atrophies in multiple skeletal muscle groups in rats. *Sci Rep* 12: 21275, 2022. doi:10.1038/s41598-022-25359-z.
  24. **Hong HK, Pyo DH, Kim TW, Yun NH, Lee YS, Song SJ, Lee WY, Cho YB.** Efficient primary culture model of patient-derived tumor cells from colorectal cancer using a Rho-associated protein kinase inhibitor and feeder cells. *Oncol Rep* 42: 2029–2038, 2019. doi:10.3892/or.2019.7285.
  25. **Jee E, Tamura Y, Kouzaki K, Kotani T, Nakazato K.** Effect of different types of muscle activity on the gene and protein expression of ALDH family members in C57BL/6J mouse skeletal muscle. *Appl Physiol Nutr Metab* 47: 775–786, 2022. doi:10.1139/apnm-2022-0005.
  26. **Schmidt EK, Clavarino G, Ceppi M, Pierre P.** SUnSET, a nonradioactive method to monitor protein synthesis. *Nat Methods* 6: 275–277, 2009. doi:10.1038/nmeth.1314.
  27. **Morales-Alcala CC, Georgiou IC, Timmis AJ, Riobo-Del Galdo NA.** Integral membrane protein 2a is a negative regulator of canonical and non-canonical hedgehog signalling. *Cells* 10: 2003, 2021. doi:10.3390/cells10082003.
  28. **Kotani T, Tamura Y, Kouzaki K, Kato H, Isemura M, Nakazato K.** Percutaneous electrical stimulation-induced muscle contraction prevents the decrease in ribosome RNA and ribosome protein during pelvic hindlimb suspension. *J Appl Physiol (1985)* 133: 822–833, 2022. doi:10.1152/jappphysiol.00204.2022.
  29. **Kasai A, Jee E, Tamura Y, Kouzaki K, Kotani T, Nakazato K.** Aldehyde dehydrogenase 2 deficiency promotes skeletal muscle atrophy in aged mice. *Am J Physiol Regul Integr Comp Physiol* 322: R511–R525, 2022. doi:10.1152/ajpregu.00304.2021.
  30. **Quiros PM, Goyal A, Jha P, Auwerx J.** Analysis of mtDNA/nDNA ratio in mice. *Curr Protoc Mouse Biol* 7: 47–54, 2017. doi:10.1002/cpmo.21.
  31. **Larionov A, Krause A, Miller WR.** A standard curve based method for relative real time PCR data processing. *BMC Bioinformatics* 6: 62, 2005. doi:10.1186/1471-2105-6-62.
  32. **Tamura Y, Kouzaki K, Kotani T, Nakazato K.** Electrically stimulated contractile activity-induced transcriptomic responses and metabolic remodeling in C<sub>2</sub>C<sub>12</sub> myotubes: twitch vs. tetanic contractions. *Am J Physiol Cell Physiol* 319: C1029–C1044, 2020. doi:10.1152/ajpcell.00494.2019.
  33. **Takahashi K, Kitaoka Y, Hatta H.** Sex-specific differences in the metabolic enzyme activity and transporter levels in mouse skeletal muscle during postnatal development. *Appl Physiol Nutr Metab* 48: 361–378, 2023. doi:10.1139/apnm-2022-0462.
  34. **Takahashi K, Kitaoka Y, Hatta H.** Effects of endurance training on metabolic enzyme activity and transporter protein levels in the skeletal muscles of orchiectomized mice. *J Physiol Sci* 72: 14, 2022. doi:10.1186/s12576-022-00839-z.
  35. **Wilson WA.** Spectrophotometric methods for the study of eukaryotic glycogen metabolism. *J Vis Exp* 174: e63046, 2021. doi:10.3797/63046-v.
  36. **Wubben TJ, Pawar M, Weh E, Smith A, Sajjakulnukit P, Zhang L, Dai L, Hager H, Pai MP, Lyssiotis CA, Besirli CG.** Small molecule activation of metabolic enzyme pyruvate kinase muscle isozyme 2, PKM2, circumvents photoreceptor apoptosis. *Sci Rep* 10: 2990, 2020. doi:10.1038/s41598-020-59999-w.
  37. **Matsunaga Y, Tamura Y, Takahashi K, Kitaoka Y, Takahashi Y, Hoshino D, Kadoguchi T, Hatta H.** Branched-chain amino acid supplementation suppresses the detraining-induced reduction of mitochondrial content in mouse skeletal muscle. *FASEB J* 36: e22628, 2022. doi:10.1096/fj.202200588R.
  38. **Muro-Pastor MI, Florencio FJ.** Purification and properties of NADP-isocitrate dehydrogenase from the unicellular cyanobacterium *Synechocystis* sp. PCC 6803. *Eur J Biochem* 203: 99–105, 1992. doi:10.1111/j.1432-1033.1992.tb19833.x.
  39. **Shi Q, Karuppagounder S, Xu H, Pechman D, Chen H, Gibson G.** Responses of the mitochondrial alpha-ketoglutarate dehydrogenase complex to thiamine deficiency may contribute to regional selective vulnerability. *Neurochem Int* 50: 921–931, 2007. doi:10.1016/j.neuint.2007.03.010.
  40. **Wakabayashi Y, Tamura Y, Kouzaki K, Kikuchi N, Hiranuma K, Menuki K, Tajima T, Yamanaka Y, Sakai A, Nakayama KI, Kawamoto T, Kitagawa K, Nakazato K.** Acetaldehyde dehydrogenase 2 deficiency increases mitochondrial reactive oxygen species emission and induces mitochondrial protease Omi/HtrA2 in skeletal muscle. *Am J Physiol Regul Integr Comp Physiol* 318: R677–R690, 2020. doi:10.1152/ajpregu.00089.2019.
  41. **Memme JM, Oliveira AN, Hood DA.** p53 regulates skeletal muscle mitochondria and mitochondrial quality control following denervation-induced muscle disuse. *J Biol Chem* 298: 101540, 2022. doi:10.1016/j.jbc.2021.101540.
  42. **Matsunaga Y, Koyama S, Takahashi K, Takahashi Y, Shinya T, Yoshida H, Hatta H.** Effects of post-exercise glucose ingestion at different solution temperatures on glycogen repletion in mice. *Physiol Rep* 9: e15041, 2021. doi:10.14814/phy2.15041.
  43. **Zhu A, Romero R, Petty HR.** A sensitive fluorimetric assay for pyruvate. *Anal Biochem* 396: 146–151, 2010. doi:10.1016/j.ab.2009.09.017.
  44. **Arai S, Kriszt R, Harada K, Looi LS, Matsuda S, Wongso D, Suo S, Ishiura S, Tseng YH, Raghunath M, Ito T, Tsuboi T, Kitaguchi T.** RGB-color intensimetric indicators to visualize spatiotemporal

- dynamics of ATP in single cells. *Angew Chem Int Ed Engl* 57: 10873–10878, 2018. doi:10.1002/anie.201804304.
45. Kimura T, Ferran B, Tsukahara Y, Shang Q, Desai S, Fedoce A, Pimentel DR, Luptak I, Adachi T, Ido Y, Matsui R, Bachschmid MM. Production of adeno-associated virus vectors for in vitro and in vivo applications. *Sci Rep* 9: 13601, 2019. doi:10.1038/s41598-019-49624-w.
  46. Chen SH, Papaneri A, Walker M, Scappini E, Keys RD, Martin NP. A simple, two-step, small-scale purification of recombinant adeno-associated viruses. *J Virol Methods* 281: 113863, 2020. doi:10.1016/j.jviromet.2020.113863.
  47. Greggio C, Jha P, Kulkarni SS, Lagarrigue S, Broskey NT, Boutant M, Wang X, Conde Alonso S, Ofori E, Auwerx J, Cantó C, Amati F. Enhanced respiratory chain supercomplex formation in response to exercise in human skeletal muscle. *Cell Metab* 25: 301–311, 2017. doi:10.1016/j.cmet.2016.11.004.
  48. Yamada T, Ashida Y, Tatebayashi D, Abe M, Himori K. Cancer cachexia induces preferential skeletal muscle myosin loss when combined with denervation. *Front Physiol* 11: 445, 2020. doi:10.3389/fphys.2020.00445.
  49. Khamoui AV, Park BS, Kim DH, Yeh MC, Oh SL, Elam ML, Jo E, Arjmandi BH, Salazar G, Grant SC, Contreras RJ, Lee WJ, Kim JS. Aerobic and resistance training dependent skeletal muscle plasticity in the colon-26 murine model of cancer cachexia. *Metabolism* 65: 685–698, 2016. doi:10.1016/j.metabol.2016.01.014.
  50. Zhuang P, Zhang J, Wang Y, Zhang M, Song L, Lu Z, Zhang L, Zhang F, Wang J, Zhang Y, Wei H, Li H. Reversal of muscle atrophy by Zhimu and Huangbai herb pair via activation of IGF-1/Akt and autophagy signal in cancer cachexia. *Support Care Cancer* 24: 1189–1198, 2016. doi:10.1007/s00520-015-2892-5.
  51. Bonetto A, Aydogdu T, Jin X, Zhang Z, Zhan R, Puzis L, Koniaris LG, Zimmers TA. JAK/STAT3 pathway inhibition blocks skeletal muscle wasting downstream of IL-6 and in experimental cancer cachexia. *Am J Physiol Endocrinol Metab* 303: E410–E421, 2012. doi:10.1152/ajpendo.00039.2012.
  52. Fujita J, Tsujinaka T, Jano M, Ebisui C, Saito H, Katsume A, Akamatsu K, Ohsugi Y, Shiozaki H, Monden M. Anti-interleukin-6 receptor antibody prevents muscle atrophy in colon-26 adenocarcinoma-bearing mice with modulation of lysosomal and ATP-ubiquitin-dependent proteolytic pathways. *Int J Cancer* 68: 637–643, 1996. doi:10.1002/(SICI)1097-0215(19961127)68:5<637::AID-IJC14>3.0.CO;2-Z.
  53. Gelin J, Moldawer LL, Lönnroth C, Sherry B, Chizzonite R, Lundholm K. Role of endogenous tumor necrosis factor  $\alpha$  and interleukin 1 for experimental tumor growth and the development of cancer cachexia. *Cancer Res* 51: 415–421, 1991.
  54. Moylan JS, Smith JD, Chambers MA, McLoughlin TJ, Reid MB. TNF induction of atrogin-1/MAFbx mRNA depends on Foxo4 expression but not AKT-Foxo1/3 signaling. *Am J Physiol Cell Physiol* 295: C986–C993, 2008. doi:10.1152/ajpcell.00041.2008.
  55. Cai D, Frantz JD, Tawa NE, Melendez PA, Oh BC, Lidov HG, Hasselgren PO, Frontera WR, Lee J, Glass DJ, Shoelson SE. IKK $\beta$ /NF- $\kappa$ B activation causes severe muscle wasting in mice. *Cell* 119: 285–298, 2004. doi:10.1016/j.cell.2004.09.027.
  56. Powrózek T, Pigoń-Zajac D, Mazurek M, Ochieng Otieno M, Rahnama-Hezavah M, Małecka-Massalska T. TNF- $\alpha$  induced myotube atrophy in C2C12 cell line uncovers putative inflammatory-related lncRNAs mediating muscle wasting. *Int J Mol Sci* 23: 3878, 2022. doi:10.3390/ijms23073878.
  57. Seto DN, Kandarian SC, Jackman RW. A key role for leukemia-inhibitory factor in C26 cancer cachexia. *J Biol Chem* 290: 19976–19986, 2015. doi:10.1074/jbc.M115.638411.
  58. Mizushima N, Yamamoto A, Matsui M, Yoshimori T, Ohsumi Y. In vivo analysis of autophagy in response to nutrient starvation using transgenic mice expressing a fluorescent autophagosome marker. *Mol Biol Cell* 15: 1101–1111, 2004. doi:10.1091/mbc.e03-09-0704.
  59. Sartori R, Romanello V, Sandri M. Mechanisms of muscle atrophy and hypertrophy: implications in health and disease. *Nat Commun* 12: 330, 2021. doi:10.1038/s41467-020-20123-1.
  60. Teslaa T, Teitell MA. Techniques to monitor glycolysis. *Methods Enzymol* 542: 91–114, 2014. doi:10.1016/B978-0-12-416618-9.00005-4.
  61. Sturm G, Karan KR, Monzel AS, Santhanam B, Taivassalo T, Bris C, Ware SA, Cross M, Towheed A, Higgins-Chen A, McManus MJ, Cardenas A, Lin J, Epel ES, Rahman S, Vissing J, Grassi B, Levine M, Horvath S, Haller RG, Lenaers G, Wallace DC, St-Onge MP, Tavazoie S, Procaccio V, Kaufman BA, Seifert EL, Hirano M, Picard M. OxPhos defects cause hypermetabolism and reduce lifespan in cells and in patients with mitochondrial diseases. *Commun Biol* 6: 22, 2023. doi:10.1038/s42003-022-04303-x.
  62. Visavadiya NP, Rossiter HB, Khamoui AV. Distinct glycolytic pathway regulation in liver, tumour and skeletal muscle of mice with cancer cachexia. *Cell Biochem Funct* 39: 802–812, 2021. doi:10.1002/cbf.3652.
  63. Yeung SJ, Pan J, Lee MH. Roles of p53, Myc and HIF-1 in regulating glycolysis—the seventh hallmark of cancer. *Cell Mol Life Sci* 65: 3981–3999, 2008. doi:10.1007/s00018-008-8224-x.
  64. Kitaoka Y, Miyazaki M, Kikuchi S. Voluntary exercise prevents abnormal muscle mitochondrial morphology in cancer cachexia mice. *Physiol Rep* 9: e15016, 2021. doi:10.14814/phy2.15016.
  65. Blackwell TA, Cervenka I, Khatri B, Brown JL, Rosa-Caldwell ME, Lee DE, Perry RA, Brown LA, Haynie WS, Wiggs MP, Bottje WG, Washington TA, Kong BC, Ruas JL, Greene NP. Transcriptomic analysis of the development of skeletal muscle atrophy in cancer cachexia in tumor-bearing mice. *Physiol Genomics* 50: 1071–1082, 2018. doi:10.1152/physiolgenomics.00061.2018.
  66. Chow LS, Gerszten RE, Taylor JM, Pedersen BK, van Praag H, Trappe S, Febbraio MA, Galis ZS, Gao Y, Haus JM, Lanza IR, Lavie CJ, Lee CH, Lucia A, Moro C, Pandey A, Robbins JM, Stanford KI, Thackray AE, Villeda S, Watt MJ, Xia A, Zierath JR, Goodpaster BH, Snyder MP. Exerkines in health, resilience and disease. *Nat Rev Endocrinol* 18: 273–289, 2022. doi:10.1038/s41574-022-00641-2.
  67. Hardee JP, Counts BR, Carson JA. Understanding the role of exercise in cancer cachexia therapy. *Am J Lifestyle Med* 13: 46–60, 2019. doi:10.1177/1559827617725283.